J|A|C|S
ARTICLES
Published on Web 04/10/2004

The Syntheses of Carbocations by Use of the Noble-Gas Oxidant, $[XeOTeF_5][Sb(OTeF_5)_6]$: The Syntheses and Characterization of the CX_3^+ (X = Cl, Br, $OTeF_5$) and $CBr(OTeF_5)_2^+$ Cations and Theoretical Studies of CX_3^+ and BX_3 (X = F, Cl, Br, I, $OTeF_5$)†

Hélène P. A. Mercier,‡ Matthew D. Moran,‡ Gary J. Schrobilgen,*,‡ Christoph Steinberg,‡ and Reijo J. Suontamo§

Contribution from the Department of Chemistry, McMaster University, Hamilton, Ontario, L8S 4M1, Canada, and Department of Chemistry, University of Jyväskylä, P.O. Box 35, FIN-40014 Jyväskylä, Finland

Received December 5, 2003; Revised Manuscript Received February 3, 2004; E-mail: schrobil@mcmaster.ca

Abstract: The CCl_3^+ and CBr_3^+ cations have been synthesized by oxidation of a halide ligand of CCl_4 and CBr_4 at −78 °C in SO_2ClF solvent by use of $[XeOTeF_5][Sb(OTeF_5)_6]$. The CBr_3^+ cation reacts further with $BrOTeF_5$ to give $CBr(OTeF_5)_2^+$, $C(OTeF_5)_3^+$, and Br_2. The $[XeOTeF_5][Sb(OTeF_5)_6]$ salt was also found to react with $BrOTeF_5$ in SO_2ClF solvent at −78 °C to give the $Br(OTeF_5)_2^+$ cation. The CCl_3^+, CBr_3^+, $CBr(OTeF_5)_2^+$, $C(OTeF_5)_3^+$, and $Br(OTeF_5)_2^+$ cations and $C(OTeF_5)_4$ have been characterized in SO_2ClF solution by ^{13}C and/or ^{19}F NMR spectroscopy at −78 °C. The X-ray crystal structures of the CCl_3^+, CBr_3^+, and $C(OTeF_5)_3^+$ cations have been determined in $[CCl_3][Sb(OTeF_5)_6]$, $[CBr_3][Sb(OTeF_5)_6]\cdot SO_2ClF$, and $[C(OTeF_5)_3][Sb(OTeF_5)_6]\cdot 3SO_2ClF$ at −173 °C. The CCl_3^+ and CBr_3^+ salts were stable at room temperature, whereas the $CBr_n(OTeF_5)_{3-n}^+$ salts were stable at 0 °C for several hours. The cations were found to be trigonal planar about carbon, with the CCl_3^+ and CBr_3^+ cations showing no significant interactions between their carbon atoms and the fluorine atoms of the $Sb(OTeF_5)_6^-$ anions. In constrast, the $C(OTeF_5)_3^+$ cation interacts with an oxygen of each of two SO_2ClF molecules by coordination along the three-fold axis of the cation. The solid-state Raman spectra of the $Sb(OTeF_5)_6^-$ salts of CCl_3^+ and CBr_3^+ have been obtained and assigned with the aid of electronic structure calculations. The CCl_3^+ cation displays a well-resolved $^{35}Cl/^{37}Cl$ isotopic pattern for the symmetric CCl_3 stretch. The energy-minimized geometries, natural charges, and natural bond orders of the CCl_3^+, CBr_3^+, CI_3^+, and $C(OTeF_5)_3^+$ cations and of the presently unknown CF_3^+ cation have been calculated using HF and MP2 methods have been compared with those of the isoelectronic BX_3 molecules (X = F, Cl, Br, I, and $OTeF_5$). The ^{13}C and ^{11}B chemical shifts for CX_3^+ (X = Cl, Br, I) and BX_3 (X = F, Cl, Br, I) were calculated by the GIAO method, and their trends were assessed in terms of paramagnetic contributions and spin−orbit coupling.

Introduction

Trihalomethyl cations, CX_3^+ (X = Cl, Br, I), have been the subject of considerable interest. The CCl_3^+ and CBr_3^+ cations have been postulated as superelectrophilic intermediates that catalyze efficient cracking, isomerization and oligomerization of alkanes and cycloalkanes, and that facilitate the syntheses of carbocations by means of hydride abstraction by the CCl_3^+ cation.[1] The CCl_3^+ cation, the first perhalomethyl cation to have been reported, has been observed in the gas phase by mass spectrometry[2] and by ion cyclotron resonance (ICR) mass spectrometry.[3] The CCl_3^+ cation has also been isolated in the solid state by ultraviolet or microwave irradiation of $CHCl_3$ and trapping of the free ion in an argon matrix at 14 K,[4,5] and by co-deposition of CCl_4 and SbF_5 on a CsI window at 77 K followed by warming to 150 K to produce $[CCl_3][Sb_2F_{10}Cl]$ in an SbF_5 matrix.[6] In all three studies, CCl_3^+ was characterized by infrared spectroscopy. The CBr_3^+ and CI_3^+ cations have been more recently observed in the gas phase by ICR mass spectrometry.[7] The CF_3^+ cation has been observed by mass

† This work has been presented, in part, at (a) the 224th National Meeting of the American Chemical Society, Neil Bartlett Symposium, Boston, MA, August 14−18, 2002 (also see Dagani, R. *Chem. Eng. News* **2002**, *80*, 27), (b) the 16th Winter Fluorine Conference, St. Petersburg Beach, FL, January 12−17, 2003, and (c) the 225th National Meeting of the American Chemical Society, Karl O. Christe Symposium, New Orleans, LA, March 23−27, 2003.

‡ Department of Chemistry, McMaster University.

§ Department of Chemistry, University of Jyväskylä.

(1) Olah, G. A.; Rasul, G.; Yudin, A. K.; Burrichter, A.; Prakash, G. K. S.; Chistyakov, A. L.; Stankevich, I. V.; Akhrem, I. S.; Gambaryan, N. P.; Vol'pin, M. E. *J. Am. Chem. Soc.* **1996**, *118*, 1446 and references therein.
(2) Martin, R. H.; Lampe, F. W.; Taft, R. W. *J. Am. Chem. Soc.* **1966**, *88*, 1353.
(3) Lias, S. G.; Eyler, J. R.; Ausloos, P. *Int. J. Mass Spectrom. Ion Phys.* **1976**, *19*, 219.
(4) Jacox, M. E.; Milligan, D. E. *J. Chem. Phys.* **1971**, *54*, 3935.
(5) Jacox, M. E. *Chem. Phys.* **1976**, *12*, 51.
(6) Vančik, H.; Percač, K.; Sunko, D. E. *J. Am. Chem. Soc.* **1990**, *112*, 7418.

spectrometry[2] and ICR mass spectrometry[3] and was first produced in the condensed state by photodecomposition of CF_3X (X = Cl, Br, I, H) in argon matrices.[8] The CF_3^+ cation has also been obtained by decomposition of an Ar/F_3CNNCF_3 mixture at 14 K that had been co-deposited with microwave-excited neon atoms[9] and by co-deposition of a Ne/CF_4 mixture at 5 K with microwave-excited neon atoms.[10] Matrix-isolated CF_3^+, derived in the aforementioned manners, was characterized by infrared spectroscopy, and the vibrational assignments for CF_3^+ have been confirmed by ab initio calculations.[11] The first syntheses of long-lived perhalomethyl cations in solution were achieved by the reactions of CX_4 (X = Cl, Br, I) with SbF_5 in SO_2ClF solvent at −78 °C to give $[CX_3][Sb_nF_{5n}X]$ (X = Cl, Br, I).[12,13] All three cations were characterized by ^{13}C NMR spectroscopy. The CCl_3^+ cation was also generated by reaction of $CCl_3C(O)Cl$, CCl_3SO_2Cl, or $CCl_3C(O)F$ with SbF_5 in SO_2ClF at −78 °C.[12,13] Similar attempts to prepare CF_3^+ by reaction of SbF_5 with CF_4, $CF_3C(O)F$, and CF_3SO_2Cl in SO_2ClF at −78 °C were unsuccessful and, in the cases of $CF_3C(O)F$ and CF_3SO_2Cl, yielded CF_4.[12,13] The CI_3^+ cation has been recently synthesized as the $[CI_3][Al(OC(CF_3)_3)_4]$ salt by the room-temperature abstraction of iodide as AgI from CI_4 in CH_2Cl_2 solution by use of $[Ag][Al(OC(CF_3)_3)_4]$ as the Ag^+ ion source, and characterized by X-ray crystallography.[14]

Peralkoxymethyl cations, $[C(OR)_3]^+$, have been extensively studied and characterized in solution and were first generated by alkylation of carbonic esters[15] and by Meerwein's method,[16,17] which involves alkoxy group abstraction from an ortho ester by BF_3. Peralkoxymethyl cations, generated in acid solutions from ortho esters or ketals, have been characterized by ultraviolet and infrared spectroscopy and by ^1H and ^{13}C NMR spectroscopy.[18] The trihydroxymethyl cation, $C(OH)_3^+$, was first generated by dissolution of M_2CO_3 (M = Na, K), $BaCO_3$, or $NaHCO_3$ in $FSO_3H-SbF_5-SO_2$ superacid solutions at −78 °C and studied by ^1H and ^{13}C NMR spectroscopy.[19] Prior to the present work, the $C(OH)_3^+$ cation was the only $C(OX)_3^+$ cation to have been isolated and studied in the solid state. The low-temperature crystal structure of $[C(OH)_3][AsF_6]$ and infrared and Raman spectra of $[C(OH)_3][MF_6]$ (M = As, Sb) were obtained by the low-temperature solvolysis of $OC(OSiMe_3)_2$ in the superacidic media HF/MF_5.[20] The salts were found to decompose quantitatively to CO_2 and $[H_3O][MF_6]$ above −16 °C (M = As) and −4 °C (M = Sb).

While a considerable number of carbocation structures have been determined by X-ray crystallography,[21] relatively few crystal structures have been determined for halogen- and oxygen-substituted carbocations. These include $[\overline{CF_2-S-CF-S}]^+$,[22] $[(CH_3)_2CF]^+$,[23] $[(m\text{-}CF_3C_6H_4)(C_6H_5)CF]^+$,[23] $[CH_3OCHF]^+$,[24] $[(o\text{-}ClC_6H_4)(C_6H_5)CCl]^+$,[25] $[ClCO]^+$,[26] $[Cl_2C{=}NH_2]^+$,[27] $[ClBrC{=}NH_2]^+$,[28] $[CH_3OCHCl]^+$,[24] $[C(OH)_2CH_3]^+$,[29,30] $[HC(OH)_2]^+$,[31] $[(C_6H_5)C(-OCH_2CH_2O-)]^+$,[32] and $[(CH_3)C(-OC(CH_3)_2C(CH_3)_2O-)]^+$.[33] Until the present work, the CI_3^+ and $C(OH)_3^+$ cations were the only perhalogen- and peroxygen-substituted cations to have been characterized by single-crystal X-ray diffraction.[14,20]

Given the relative paucity of solid-state structural data for trihalomethyl cations, electronic structure calculations have been heavily relied upon for metric data and have been used to account for the bonding and chemical properties of these cations. The relative stabilities of the trihalomethyl cations have been assessed in terms of relative degrees of σ and $p(\pi)$ donation from the halogen atom to the carbon center.[13,14,23,26,34−36] The σ effect, from the perspective of the halogen atoms of CX_3^+, has been found to be strongly withdrawing in the case of fluorine and weakly donating in the cases of chlorine, bromine, and iodine (I > Br > Cl). Conversely, $p(\pi)$ back-donation is very weak for fluorine and stronger for the heavier halogens (I > Br > Cl). Other properties also have been computed for the CX_3^+ series, including ^{13}C chemical shifts,[37] fluoride ion affinities (as measures of relative Lewis acidities),[14] vibrational frequencies,[11] and atomic charges.[13,14,23,26,34−36]

While prior syntheses of long-lived perhalomethyl cations have been achieved by halide ion abstraction by use of either a strong Lewis acid or Ag^+ (vide supra), no routes to such carbocations through oxidative removal of a halogen bound to carbon were known. Among the objectives of the present work are to provide structural and spectroscopic data for the perhalomethyl cations and related $OTeF_5$-substituted cations that, thus far, have been lacking for these systems. The present paper details an oxidative route to carbocations using the strongly oxidizing salt, $[XeOTeF_5][Sb(OTeF_5)_6]$, and represents an interesting new application of noble-gas compounds to chemical syntheses.[38−40] The present solution, solid-state, and computa-

(7) Abboud, J.-L. M.; Castaño, O.; Herreros, M.; Elguero, J.; Jagerovic, N.; Notario, R.; Sak, K. *Int. J. Mass Spectrom. Ion Proc.* **1998**, *175*, 35.
(8) Prochaska, F. T.; Andrews, L. *J. Am. Chem. Soc.* **1978**, *100*, 2102.
(9) Jacox, M. E. *Chem. Phys.* **1984**, *83*, 171.
(10) Forney, D.; Jacox, M. E.; Irikura, K. K. *J. Chem. Phys.* **1994**, *101*, 8290.
(11) Maclagan, R. G. A. R. *J. Mol. Struct. (THEOCHEM)* **1991**, *235*, 21.
(12) Olah, G. A.; Heiliger, L.; Prakash, G. K. S. *J. Am. Chem. Soc.* **1989**, *111*, 8020.
(13) Olah, G. A.; Rasul, G.; Heiliger, L.; Prakash, G. K. S. *J. Am. Chem. Soc.* **1996**, *118*, 3580.
(14) Krossing, I.; Bihlmeier, A.; Raabe, I.; Trapp, N. *Angew. Chem., Int. Ed.* **2003**, *42*, 1531.
(15) Klages, F.; Zange, E. *Chem. Ber.* **1959**, *92*, 1828.
(16) Meerwein, H.; Bodenbenner, K.; Borner, P.; Kunert, F.; Wunderlich, H. *Ann.* **1960**, *632*, 38.
(17) Meerwein, H.; Hederich, V.; Morschel, H.; Wunderlich, H. *Ann.* **1960**, *635*, 1.
(18) Ramsey, B. G.; Taft, R. W. *J. Am. Chem. Soc.* **1966**, *88*, 3058.
(19) Olah, G. A.; White, A. M. *J. Am. Chem. Soc.* **1968**, *90*, 1884.
(20) Minkwitz, R.; Schneider, S. *Angew. Chem., Int. Ed.* **1999**, *38*, 714.
(21) Laube, T. *Chem. Rev.* **1998**, *98*, 1277 and references therein.
(22) Antel, J.; Klaus, H.; Jones, P. G.; Mews, R.; Sheldrick, G. M.; Waterfeld, A. *Chem. Ber.* **1985**, *118*, 5006.
(23) Christe, K. O.; Zhang, X.; Bau, R.; Hegge, J.; Olah, G. A.; Prakash, G. K. S.; Sheehy, J. A. *J. Am. Chem. Soc.* **2000**, *122*, 481.
(24) Minkwitz, R.; Reinemann, S.; Blecher, O.; Hartl, H.; Brüdgam, I. *Inorg. Chem.* **1999**, *38*, 844.
(25) Laube, T.; Bannwart, E.; Hollenstein, S. *J. Am. Chem. Soc.* **1993**, *115*, 1731.
(26) Christe, K. O.; Hoge, B.; Boatz, J. A.; Prakash, G. K. S.; Olah, G. A.; Sheehy, J. A. *Inorg. Chem.* **1999**, *38*, 3132.
(27) Minkwitz, R.; Meckstroth, W.; Preut, H. *Z. Anorg. Allg. Chem.* **1992**, *617*, 136.
(28) Minkwitz, R.; Meckstroth, W.; Preut, H. *Z. Naturforsch., B: Chem. Sci.* **1992**, *48*, 19.
(29) Jönsson, P.-G.; Olovsson, I. *Acta Crystallogr.* **1968**, *B24*, 559.
(30) Kvick, Å.; Jönsson, P.-G.; Olovsson, I. *Inorg. Chem.* **1969**, *8*, 2775.
(31) Minkwitz, R.; Schneider, S.; Seifert, M. *Z. Anorg. Allg. Chem.* **1996**, *622*, 1404.
(32) Caira, M. R.; De Wet, J. F. *Acta Crystallogr.* **1981**, *B37*, 709.
(33) Paulsen, H.; Dammeyer, R. *Chem. Ber.* **1973**, *106*, 2324.
(34) Frenking, G.; Fau, S.; Marchand, C. M.; Grützmacher, H. *J. Am. Chem. Soc.* **1997**, *119*, 6648.
(35) Robinson, E. A.; Johnson, S. A.; Tang, T.-H.; Gillespie, R. J. *Inorg. Chem.* **1997**, *36*, 3022.
(36) Robinson, E. A.; Heard, G. L.; Gillespie, R. J. *J. Mol. Struct.* **1999**, *485−486*, 305.
(37) Kaupp, M.; Malkina, O. L.; Malkin, V. G. *Chem. Phys. Lett.* **1997**, *265*, 55.
(38) Minkwitz, R.; Bäck, B. In *Inorganic Fluorine Chemistry, Toward the 21st Century*; Thrasher, J. S., Strauss, S. H., Eds.; ACS Symposium Series 555; American Chemical Society: Washington, DC, 1994; Chapter 6, p 90.
(39) Brown, D. R.; Clegg, M. J.; Downs, A. J.; Fowler, R. C.; Minihan, A. R.; Norris, J. R.; Stein, L. *Inorg. Chem.* **1992**, *31*, 5041.

Table 1. ^{13}C and ^{19}F NMR Parameters[a] for $C(OTeF_5)_4$ and $CBr_n(OTeF_5)_{3-n}^+$ ($n = 0-3$) and Products Resulting from the Reaction of $[XeOTeF_5][Sb(OTeF_5)_6]$ with CCl_4 and CBr_4

	chem shift (δ), ppm[b]			coupling constant, Hz[b]						100 × (total satellite intens/central peak intens)[c]
species	^{13}C	$^{19}F_B$	$^{19}F_A$	$^2J(^{13}C-^{125}Te)$	$^2J(^{19}F_A-^{19}F_B)$	$^1J(^{19}F_B-^{125}Te)$	$^1J(^{19}F_A-^{125}Te)$	$^1J(^{19}F_B-^{123}Te)$	$^1J(^{19}F_A-^{123}Te)$	^{125}Te
CCl_3^+ [d]	237.1									
CBr_3^+ [d]	209.7									
$CBr_2(OTeF_5)^+$ [d]	201.1[e]	−19.9	−61.3		156	4099				
$CBr(OTeF_5)_2^+$ [d]	187.6	−24.4	−59.3		162	4029	4075	3343		
$C(OTeF_5)_3^+$ [d]	168.8	−31.6	−57.6	69	164	4025	4012	3337		12 ± 1 (12.7)
$C(OTeF_5)_4$	115.8	−41.5	−49.9	64	180	3758	3653	3120	3029	16.9 ± 0.1 (16.8)
$Br(OTeF_5)_2^+$ [d]		−24.4	−58.2		164	4013	4047	3324	3350	
$BrOTeF_5$ [f]		−53.8	−47.0		180	3786	3419	3140		
$ClOTeF_5$		−54.0	−49.2		178	3852	3474			
$Sb(OTeF_5)_6^-$ [d]		−42.6				3563				

[a] Nuclear magnetic resonance spectra were obtained for SO_2ClF solutions at −80 °C ($\delta(^{19}F)$, 98.3 ppm; primary and secondary isotope shifts: $^2\Delta^{19}F(^{16/18}O)$, 0.0428 ppm, $^1\Delta^{19}F(^{32/34}S)$, 0.0611 ppm, and $^2\Delta^{19}F(^{35/37}Cl)$, 0.0085 ppm. [b] The symbols, F_A and F_B, denote equatorial and axial fluorine atoms, respectively. [c] Ratios calculated from natural isotopic abundances are given in parentheses. [d] The $Sb(OTeF_5)_6^-$ anion parameters apply to all carbocation salts and to the $Br(OTeF_5)_2^+$ salt of $Sb(OTeF_5)_6^-$; also see ref 41. [e] Predicted from pairwise additivity parameters as described in the Chemical Shifts and Coupling Constant Trends section. [f] See refs 42 and 43.

tional studies compliment previous solution ^{13}C NMR studies of the CCl_3^+, CBr_3^+, and CI_3^+ [12−14] cations, as well as the X-ray structure of the CI_3^+ cation,[14] which followed our preliminary accounts of the present work.[†]

Results and Discussion

Syntheses of $[CCl_3][Sb(OTeF_5)_6]$, $[CBr_n(OTeF_5)_{3-n}][Sb(OTeF_5)_6]$ ($n = 0, 1, 3$), $[Br(OTeF_5)_2][Sb(OTeF_5)_6]$, and $C(OTeF_5)_4$ and Solution Characterization by ^{19}F and ^{13}C NMR Spectroscopy. The products of the reactions described below were initially characterized in SO_2ClF solution by ^{13}C and ^{19}F NMR spectroscopy, and their NMR parameters are provided in Table 1.

The synthesis and X-ray crystal structure of $[XeOTeF_5][Sb(OTeF_5)_6]\cdot SO_2ClF$ will be described in a forthcoming publication.[44] Unlike that of its fluorine analogue, $[XeF][SbF_6]$, which is insoluble in SO_2ClF at room temperature, the solubility of $[XeOTeF_5][Sb(OTeF_5)_6]$ in SO_2ClF exceeds 2 M at −78 °C, forming an intense yellow solution. The salt rapidly oxidizes stoichiometric amounts of CCl_4 at −78 °C to yield clear, colorless solutions of $[CCl_3][Sb(OTeF_5)_6]$ according to eq 1.

$$[XeOTeF_5][Sb(OTeF_5)_6] + CCl_4 \rightarrow [CCl_3][Sb(OTeF_5)_6] + ClOTeF_5 + Xe \quad (1)$$

Removal of SO_2ClF and other volatile components under vacuum between −78 and 0 °C gave colorless, crystalline $[CCl_3][Sb(OTeF_5)_6]$ (see X-ray Crystallography), which was found to be stable indefinitely at room temperature.

The ^{13}C NMR spectrum (SO_2ClF solvent, −80 °C) of the products resulting from eq 1 give rise to a sharp singlet (237.1 ppm) assigned to $[CCl_3][Sb(OTeF_5)_6]$, which is in agreement with the previously reported value (236.3 ppm).[12] The ^{13}C chemical shift of CCl_3^+ is significantly deshielded relative to that of CCl_4 [$\delta(^{13}C)$, 96.4 ppm; SO_2ClF, −80 °C], which is consistent with carbocation formation (see Chemical Shift and Coupling Constant Trends). The ^{19}F NMR spectrum shows the severe AB_4 pattern that typifies the $Sb(OTeF_5)_6^-$ anion[41] and a well-resolved AB_4 pattern for $ClOTeF_5$ (Table 1).[45]

The reaction of stoichiometric amounts of CBr_4 with $[XeOTeF_5][Sb(OTeF_5)_6]$ in SO_2ClF is initially rapid at −78 °C, giving a deep red-brown solution which lightens to red-orange over a period of several hours at ca. −50 °C. The color change corresponds to the further reaction of the CBr_3^+ cation with $BrOTeF_5$ to produce Br_2 and the mixed carbocations, $CBr_2(OTeF_5)^+$, $CBr(OTeF_5)_2^+$, and ultimately $C(OTeF_5)_3^+$, according to eqs 2−5, with the overall reaction being represented by eq 6.

$$3[XeOTeF_5][Sb(OTeF_5)_6] + 3CBr_4 \rightarrow 3[CBr_3][Sb(OTeF_5)_6] + 3BrOTeF_5 + 3\,Xe \quad (2)$$

$$[CBr_3][Sb(OTeF_5)_6] + BrOTeF_5 \rightarrow [CBr_2(OTeF_5)][Sb(OTeF_5)_6] + Br_2 \quad (3)$$

$$[CBr_2(OTeF_5)][Sb(OTeF_5)_6] + BrOTeF_5 \rightarrow [CBr(OTeF_5)_2][Sb(OTeF_5)_6] + Br_2 \quad (4)$$

$$[CBr(OTeF_5)_2][Sb(OTeF_5)_6] + BrOTeF_5 \rightarrow [C(OTeF_5)_3][Sb(OTeF_5)_6] + Br_2 \quad (5)$$

$$3[XeOTeF_5][Sb(OTeF_5)_6] + 3CBr_4 \rightarrow 2[CBr_3][Sb(OTeF_5)_6] + [C(OTeF_5)_3][Sb(OTeF_5)_6] + 3Br_2 + 3\,Xe \quad (6)$$

Removal of SO_2ClF and other volatile components under vacuum between −78 and 0 °C resulted in a pale, yellow-orange solid. The Raman spectra of the solid mixture showed that the CBr_3^+ salt was stable indefinitely at room temperature, whereas the mixed $CBr_n(OTeF_5)_{3-n}^+$ salts were stable for several hours at 0 °C. The $[CBr_3][Sb(OTeF_5)_6]$ and $[C(OTeF_5)_3][Sb(OTeF_5)_6]$ salts have been characterized by single-crystal X-ray diffraction, and Br_2 was identified by determination of the unit cell parameters from a single crystal at −173 °C (see Experimental Section).

(40) Frohn, H.-J.; Klose, A.; Henkel, G. *GIT Fachz. Lab.* **1993**, *37*, 752.
(41) Mercier, H. P. A.; Sanders, J. C. P.; Schrobilgen, G. J. *J. Am. Chem. Soc.* **1994**, *116*, 2921.
(42) Seppelt, K. *Chem. Ber.* **1973**, *106*, 1920.
(43) Gerken, M.; Kolb, P.; Wegner, A.; Mercier, H. P. A.; Borrmann, H.; Dixon, D. A.; Schrobilgen, G. J. *Inorg. Chem.* **2000**, *39*, 2813.
(44) Mercier, H. P. A.; Moran, M. D.; Sanders, J. C. P.; Schrobilgen, G. J.; Suontamo, R. J. To be submitted for publication.
(45) Seppelt, K. *Z. Anorg. Allg. Chem.* **1973**, *399*, 65.

The ^{13}C NMR spectrum of $[CBr_3][Sb(OTeF_5)_6]$ in SO_2ClF at −80 °C gave rise to a singlet (209.7 ppm), in good agreement with the previously reported value (207 ppm).[12] As in the case of CCl_3^+, the ^{13}C resonance of CBr_3^+ is significantly deshielded with respect to that of its parent molecule, CBr_4 [$\delta(^{13}C)$, −29.7 ppm; SO_2ClF, −80 °C], which is characteristic of carbocation formation (see Chemical Shift and Coupling Constant Trends). The ^{19}F NMR spectrum shows a severe AB_4 pattern corresponding to the $Sb(OTeF_5)_6^-$ anion (Table 1), similar to that obtained for $[CCl_3][Sb(OTeF_5)_6]$. The ^{19}F NMR spectrum of a sample of pure $BrOTeF_5$ dissolved in SO_2ClF at −80 °C (Table 1) was also obtained and demonstrated that $BrOTeF_5$, as proposed in eq 2, was not present. The absence of $BrOTeF_5$ is consistent with the formation of mixed Br/$OTeF_5$-substituted methyl cations and the oxidation of $BrOTeF_5$ by $[XeOTeF_5][Sb(OTeF_5)_6]$ to give the new $Br(OTeF_5)_2^+$ cation (eq 7).

$$[XeOTeF_5][Sb(OTeF_5)_6] + BrOTeF_5 \rightarrow [Br(OTeF_5)_2][Sb(OTeF_5)_6] + Xe \quad (7)$$

The formation of $Br(OTeF_5)_2^+$ was confirmed by reaction of $BrOTeF_5$ with $[XeOTeF_5][Sb(OTeF_5)_6]$ in SO_2ClF at −78 °C in a separate experiment.[46]

The formation of the $CBr_n(OTeF_5)_{3-n}^+$ ($n = 1-3$) cations and their NMR assignments were confirmed by addition of $BrOTeF_5$ at −20 °C to the reaction products of eq 6, in a 3:1 molar ratio relative to the initial amounts of $[XeOTeF_5][Sb(OTeF_5)_6]$ and CBr_4. This resulted in increased amounts of the $OTeF_5$-containing carbocations and Br_2 as outlined in eqs 3−5 (Table 1). The ^{13}C NMR spectrum indicated that a small quantity of $[CBr_3][Sb(OTeF_5)_6]$ remained unreacted (7% based on integration of all ^{13}C resonances) with $[C(OTeF_5)_3][Sb(OTeF_5)_6]$ as the major product (70%; $\delta(^{13}C)$, 168.8 ppm). Of the mixed $OTeF_5$-substituted bromocations, $CBr_n(OTeF_5)_{3-n}^+$ ($n = 1, 2$), only the $CBr(OTeF_5)_2^+$ cation was detected by ^{13}C NMR spectroscopy (10%; $\delta(^{13}C)$, 187.6 ppm), while the ^{13}C chemical shift of $CBr_2(OTeF_5)^+$ was predicted by use of pairwise additivity parameters ($\delta(^{13}C)$, 201.1 ppm; see Chemical Shift and Coupling Constant Trends). A singlet was also observed (13%; $\delta(^{13}C)$, 124.7 ppm) that is tentatively assigned to $O{=}C(OTeF_5)_2$ based on the similarity of its ^{13}C chemical shift to that of $O{=}CF_2$ (134.2 ppm)[47] and may arise from the formal loss of the TeF_5^+ cation from $C(OTeF_5)_3^+$, according to eq 8. Alternatively, $O{=}C(OTeF_5)_2$ may prove to be unstable, decomposing to CO_2 ($\delta(^{13}C)$, 124.2 ppm)[48] and $O(TeF_5)_2$ [$\delta(^{19}F_B)$, −41.4 ppm; F_A was not observed because of overlap with F_A of $C(OTeF_5)_3^+$; $^2J(^{19}F_B-^{19}F_A)$, 164 Hz] according to eq 9.

$$[C(OTeF_5)_3][Sb(OTeF_5)_6] \rightarrow O{=}C(OTeF_5)_2 + [TeF_5][Sb(OTeF_5)_6] \quad (8)$$

$$O{=}C(OTeF_5)_2 \rightarrow CO_2 + O(TeF_5)_2 \quad (9)$$

The TeF_5^+ cation presumably was not observed because of its high electrophilicity, which could lead to $OTeF_5^-$ abstraction from $Sb(OTeF_5)_6^-$, forming $O(TeF_5)_2$ according to eq 10 and/or F^- abstraction to form TeF_6 [$\delta(^{19}F)$, −52.6 ppm; $^1J(^{19}F-^{125}Te)$, 3747 Hz; $^1J(^{19}F-^{123}Te)$, 3095 Hz] according to eq 11. The proposed species, $Sb(OTeF_5)_5$, which is known to be unstable,[49,50] and $F_4TeOSb(OTeF_5)_5$ have not been investigated further in this study.

$$[TeF_5][Sb(OTeF_5)_6] \rightarrow O(TeF_5)_2 + Sb(OTeF_5)_5 \quad (10)$$

$$[TeF_5][Sb(OTeF_5)_6] \rightarrow TeF_6 + F_4TeOSb(OTeF_5)_5 \quad (11)$$

The formation of the $C(OTeF_5)_3^+$ cation was confirmed by the presence of a $^{123/125}Te$ satellite doublet in the ^{13}C NMR spectrum [$^2J(^{13}C-^{125}Te)$, 69 Hz].[51] The similar gyromagnetic ratios of ^{123}Te and ^{125}Te and the low natural abundance of ^{123}Te (0.87%) relative to ^{125}Te (6.99%) precluded the observation of separate ^{123}Te satellites because of overlap with the more intense ^{125}Te satellites ($\nu_{1/2} \approx 5$ Hz). By combining the intensities expected for coupling to ^{123}Te and ^{125}Te, the integrated satellite peak/central peak intensity ratios 0.111:1.000:0.123 in the ^{13}C NMR spectrum were shown to be consistent with the calculated satellite peak/central peak intensity ratios 0.0001:0.0054:0.1268:1.0000:0.1268:0.0054:0.0001 expected for a series of overlapping isotopomer subspectra that correspond to three chemically equivalent tellurium atoms.[52] Tellurium satellites were not observed for $CBr(OTeF_5)_2^+$, owing to the low concentration of this species (10%).

To compare the NMR parameters of $C(OTeF_5)_3^+$ with those of the unknown neutral parent, $C(OTeF_5)_4$, CBr_4 was allowed to react with a stoichiometric amount of $BrOTeF_5$ at −78 °C according to eq 12.

$$CBr_4 + 4\ BrOTeF_5 \rightarrow C(OTeF_5)_4 + 4\ Br_2 \quad (12)$$

The ^{13}C NMR resonance of $C(OTeF_5)_4$ is a singlet at 115.8 ppm, accompanied by $^{123/125}Te$ satellites. As expected, the ^{13}C chemical shift of $C(OTeF_5)_4$ is significantly shielded with respect to that of the $C(OTeF_5)_3^+$ cation. As in the case of $C(OTeF_5)_3^+$, the formation of $C(OTeF_5)_4$ was confirmed by the relative intensities of the overlapping $^{123/125}Te$ satellites that arise from the natural abundance tellurium isotopomers [$^2J(^{13}C-^{125}Te)$, 64 Hz].[53] The integrated satellite peak/central peak area ratios of 0.168:1.000:0.170 in the ^{13}C NMR spectrum confirm coupling to four chemically equivalent tellurium atoms when compared with the calculated intensity ratios (3×10^{-6}: 0.0003:0.0107:0.1678:1.0000:0.1678:0.0107:0.0003:3×10^{-6}).

X-ray Crystal Structures of $[CCl_3][Sb(OTeF_5)_6]$, $[CBr_3][Sb(OTeF_5)_6]\cdot SO_2ClF$, and $[C(OTeF_5)_3][Sb(OTeF_5)_6]\cdot 3SO_2ClF$. Details of data collection parameters and other crystallographic information are provided in Table 2. Bond lengths and bond angles for the CCl_3^+, CBr_3^+, and $C(OTeF_5)_3^+$ cations are listed in Table 3. Closest secondary contacts between the carbon and halogen atoms of the cations and the fluorine atoms of the anion or oxygen atoms of the SO_2ClF solvent molecules are also given

(46) Mercier, H. P. A.; Moran, M. D.; Schrobilgen, G. J.; Suontamo, R. J. To be submitted for publication.
(47) Gombler, W. *Spectrochim. Acta, Part A* **1981**, *37*, 57.
(48) Ettinger, R.; Blume, P.; Patterson, A.; Lauterbur, P. C. *J. Magn. Reson.* **1972**, *33*, 1597.
(49) Lentz, D.; Seppelt, K. *Z. Anorg. Allg. Chem.* **1983**, *502*, 83.
(50) Syvret, R. G.; Mitchell, K. M.; Sanders, J. C. P.; Schrobilgen, G. J. *Inorg. Chem.* **1992**, *31*, 3381.
(51) Using $^nJ_{AB} = (\gamma_A{}^nJ_{A'B}/\gamma_{A'})$, the calculated value for $^1J(^{19}F-^{123}Te)$ is 57 Hz.
(52) Sanders, J. C. P.; Schrobilgen, G. J. In *Proceedings of the NATO Advanced Study Institute on Methodological Approach to Multinuclear NMR in Liquids and Solids − Chemical Applications*; Granger, P., Harris, R. K., Eds.; Kluwer Academic Publishers: Dordrecht, The Netherlands, 1988; Vol. 322, pp 160−166.
(53) The calculated value for $^1J(^{19}F-^{123}Te)$ is 53 Hz; see ref 51.

Table 2. Crystallographic Data for $[CCl_3][Sb(OTeF_5)_6]$, $[CBr_3][Sb(OTeF_5)_6]\cdot SO_2ClF$, and $[C(OTeF_5)_3][Sb(OTeF_5)_6]\cdot 3SO_2ClF$

	CCl_3^+	$C(OTeF_5)_3^+$	CBr_3^+
chem formula	$CCl_3F_{30}O_6SbTe_6$	$CCl_3F_{48}O_{15}S_3SbTe_9$	$CClBr_3F_{31}O_8SSbTe_6$
space group	$P\bar{1}$	$P\bar{1}$	$P2_1/n$
a (Å)	8.706(2)	10.082(4)	18.617(6)
b (Å)	9.181(2)	10.950(4)	9.935(3)
c (Å)	9.862(2)	24.572(10)	19.129(7)
α (deg)	104.111(5)	83.482(8)	90
β (deg)	103.507(5)	81.679(7)	90.781(7)
γ (deg)	98.851(5)	70.019(7)	90
V (Å^3)	724.5(5)	2517(3)	3538(4)
molecules/unit cell	1	2	4
mol wt (g mol^{-1})	1671.71	5273.38	7694.40
calcd density (g cm^{-3})	3.832	3.480	3.611
T (°C)	−173	−173	−173
μ (cm^{-1})	73.7	61.7	93.5
R_1[a]	0.0355	0.0668	0.0621
wR_2[b]	0.0736	0.1259	0.1211

[a] R_1 is defined as $\Sigma||F_o| - |F_c||/\Sigma|F_o|$ for $I > 2\sigma(I)$; wR_2 is defined as $[\Sigma[w(F_o^2 - F_c^2)^2]/\Sigma w(F_o^2)^2]^{1/2}$ for $I > 2\sigma(I)$.

in Table 3 together with important bond lengths and bond angles for the $Sb(OTeF_5)_6^-$ anions and SO_2ClF solvent molecules. A complete list of bond lengths and bond angles for the $Sb(OTeF_5)_6^-$ anions and SO_2ClF solvent molecules is also provided (Supporting Information).

The present contribution reports the first crystal structures of the CCl_3^+, CBr_3^+, and $C(OTeF_5)_3^+$ cations. The $Sb(OTeF_5)_6^-$ anion, which has been described previously,[41,54] is comprised of a central antimony atom coordinated to six oxygen atoms, and each of the six tellurium atoms is octahedrally coordinated to one oxygen and five fluorine atoms so that the anion structure can be described as an octahedron of octahedra. Bond angles and bond lengths of the $Sb(OTeF_5)_6^-$ anions reported in the present study are in good agreement with those reported in the crystal structures of $[SbBr_4][Sb(OTeF_5)_6]$,[54] $[SbCl_4][Sb(OTeF_5)_6]$,[54] $[N(CH_3)_4][Sb(OTeF_5)_6]$,[41] and $[N(CH_2CH_3)_4][Sb(OTeF_5)_6]$,[41] and therefore require no further comment. The SO_2ClF solvent molecules present in the structures of $[CBr_3][Sb(OTeF_5)_6]\cdot SO_2ClF$ and $[C(OTeF_5)_3][Sb(OTeF_5)_6]\cdot 3SO_2ClF$ have the expected pseudotetrahedral geometry, with the S−O, S−Cl, and S−F bond lengths in agreement with those obtained from the X-ray crystal structure of SO_2ClF[55] and require no further comment (Table 3). There are no significant differences between the metric parameters of the two coordinated and one uncoordinated SO_2ClF molecule in the $[C(OTeF_5)_3][Sb(OTeF_5)_6]\cdot 3SO_2ClF$ structure.

(a) $[CCl_3][Sb(OTeF_5)_6]$ and $[CBr_3][Sb(OTeF_5)_6]\cdot SO_2ClF$. The trigonal planar CCl_3^+ cation in $[CCl_3][Sb(OTeF_5)_6]$ is positionally two-fold disordered about the crystallographic inversion center (Figure 1), contrasting with the CBr_3^+ cation in $[CBr_3][Sb(OTeF_5)_6]\cdot SO_2ClF$ which is not disordered (Figure 2). In both cases, the three halogen atoms are crystallographically independent, and carbocation planarity is not imposed by symmetry, with X−C−X bond angle sums of 360(1)°. The C−Br bond lengths and Br−C−Br angles of CBr_3^+ are all equal within $\pm 3\sigma$, giving the expected D_{3h} symmetry. As a consequence of the disorder, the CCl_3^+ cation gives a slightly wider range of bond lengths and angles, but displays essentially D_{3h} symmetry in its crystal structure. The C−Cl and C−Br bond lengths are found to be shorter than in CCl_4 (1.751(13) Å),[56] $CFCl_3$ (1.75(1) Å)[57] and CBr_4 (1.91(4) Å)[58] by ca. 0.15, 0.13, and 0.10 Å, respectively, as expected for cations (see Computational Results for CX_3^+ and BX_3). In the case of the previously reported structures of chloro- and bromo-substituted carbocations, the C−Cl or C−Br bond lengths are marginally longer than in CCl_3^+ and CBr_3^+, i.e., $[(o\text{-}ClC_6H_4)(C_6H_5)CCl][SbF_6]$[25] (C−Cl, 1.668(8) Å), $[Cl_2C{=}NH_2][SbCl_6]$[27] (C−Cl, 1.663(6)-1.680(6) Å), $[CH_3OCHCl][SbF_6]$[24] (C−Cl, 1.650(9) Å), and $[ClBrC{=}NH_2][SbCl_6]$[28] (C−Cl, 1.69(1); C−Br, 1.843(9) Å). In the CCl_3^+ and CBr_3^+ salts, the shortest cation−anion C···F contacts are 2.962(9) Å and 3.09(2) Å, respectively, (cf. the sum of the carbon and fluorine van der Waals radii, 3.10,[59] 3.30[60] Å). These contacts approach the carbon at angles of 3° (CCl_3^+) and 8° (CBr_3^+) with respect to the C_3-axis. As well, longer C···F contacts (CCl_3^+, 3.464(9), 3.574(11), and 3.574-(11) Å; CBr_3^+, 3.39(2) Å) approach above and below the CX_3-plane at angles of 4, 13, and 37° (CCl_3^+) and 8° (CBr_3^+), respectively. The bond length and bond angle trends are consistent with the previously noted trend of decreasing contact angle with decreasing contact distance in a number of carbocation structures.[21] The present structures indicate that the $Sb(OTeF_5)_6^-$ anions are very weakly coordinated to the carbon centers. The occurrence of cation−anion contacts is a common feature, and the present C···F contact distances are comparable to those observed in $[CI_3][Al(OC(CF_3)_3\}_4]$[14] (the shortest is 3.26 Å) and in $[(m\text{-}CF_3C_6H_4)(C_6H_5)CF][As_2F_{11}]$ (3.01(2) and 3.07-(2) Å).[23] The chlorine and bromine atoms also interact with the fluorine atoms of the anion and, in the case of the CBr_3^+ salt, with the oxygen atoms of SO_2ClF (Cl···F: 2.833(5)−3.022(5) Å; Br···F: 2.977(9)−3.301(11) Å; Br···O: 2.778(13), 2.839-(12) Å). These interactions are shorter than or are at the limit of the sum of the halogen−fluorine(oxygen) van der Waals radii (Cl···F, 3.15,[59] 3.22[60] Å; Br···F, 3.30,[59] 3.32[60] Å; Br···O, 3.35,[59] 3.37[60] Å) and are apparently a consequence of the positive charges on the halogen atoms (see Computational Results for CX_3^+ and BX_3). The Br···O contacts, which occur with the oxygen atoms of two SO_2ClF solvent molecules, are shorter than the secondary C···F cation−anion contacts in the CCl_3^+

(54) Casteel, W. J.; Kolb, P.; LeBlond, N.; Mercier, H. P. A.; Schrobilgen, G. J. *Inorg. Chem.* **1996**, *35*, 929.
(55) Mootz, D.; Merschenz-Quack, A. *Acta Crystallogr.* **1988**, *C44*, 924.
(56) Cohen, S.; Powers, R.; Rudman, R. *Acta Crystallogr.* **1979**, *B35*, 1670.
(57) Cockcroft, J. K.; Fitch, A. N. *Z. Kristallogr.* **1994**, *209*, 488.
(58) More, M.; Baert, F.; Lefebvre, J. *Acta Crystallogr.* **1977**, *B33*, 3681.
(59) Pauling, L., *The Nature of the Chemical Bond*, 3rd ed.; Cornell University Press: Ithaca, New York, 1960, 260.
(60) Bondi, A. *J. Phys. Chem.* **1964**, *68*, 441.

Table 3. Experimental Geometries in $[CCl_3][Sb(OTeF_5)_6]$, $[CBr_3][Sb(OTeF_5)_6]\cdot SO_2ClF$, and $[C(OTeF_5)_3][Sb(OTeF_5)_6]\cdot 3SO_2ClF$

$[CCl_3][Sb(OTeF_5)_6]$

bond lengths (Å)		bond angles (deg)	
C(1)−Cl(1)	1.672(11)	Cl(1)−C(1)−Cl(2)	118.4(8)
C(1)−Cl(2)	1.598(12)	Cl(1)−C(1)−Cl(3)	118.7(7)
C(1)−Cl(3)	1.592(13)	Cl(2)−C(1)−Cl(3)	123.3(8)
C(1)···F(14A)	2.962(9) [3°][a]		
C(1)···F(14)	3.464(9) [4°][a]		
C(1)···F(8A)	3.574(11) [13°][a]		
C(1)···F(2A)	3.574(11) [37°][a]		

$[CBr_3[Sb(OTeF_5)_6]\cdot SO_2ClF$

bond lengths (Å)		bond angles (deg)	
C(1)−Br(1)	1.851(16)	Br(1)−C(1)−Br(2)	119.1(9)
C(1)−Br(2)	1.787(16)	Br(1)−C(1)−Br(3)	117.9(9)
C(1)−Br(3)	1.783(16)	Br(2)−C(1)−Br(3)	122.9(9)
C(1)···F(44A)	3.39(2) [8°][a]		
C(1)···F(24A)	3.09(2) [8°][a]		

$C(OTeF_5)_3[Sb(OTeF_5)_6]\cdot 3SO_2ClF$

bond lengths (Å)					
C(1)−O(1)	1.313(16)	C(1)−O(2)	1.279(13)	C(1)−O(3)	1.258(15)
Te(1)−O(1)	1.988(7)	Te(2)−O(2)	1.974(8)	Te(3)−O(3)	1.977(9)
Te(1)−F(1)	1.816(6)	Te(2)−F(6)	1.798(8)	Te(3)−F(11)	1.819(8)
Te(1)−F(2)	1.816(8)	Te(2)−F(7)	1.812(8)	Te(3)−F(12)	1.795(8)
Te(1)−F(3)	1.801(8)	Te(2)−F(8)	1.810(7)	Te(3)−F(13)	1.820(6)
Te(1)−F(4)	1.813(8)	Te(2)−F(9)	1.816(9)	Te(3)−F(14)	1.799(6)
Te(1)−F(5)	1.814(8)	Te(2)−F(10)	1.808(8)	Te(3)−F(15)	1.809(8)
C(1)···O(11)	2.690(17) [1°][a]	C(1)···O(15A)	2.738(18) [3°][a]		

bond angles (deg)					
O(1)−C(1)−O(2)	119(1)	O(1)−C(1)−O(3)	119.8(9)	O(2)−C(1)−O(3)	121(1)
C(1)−O(1)−Te(1)	125.5(7)	C(1)−O(2)−Te(2)	132.7(9)	C(1)−O(3)−Te(3)	131.2(8)
O(1)−Te(1)−F(1)	176.8(4)	O(2)−Te(2)−F(6)	176.2(4)	O(3)−Te(3)−F(11)	174.6(3)
O(1)−Te(1)−F(2)	91.2(3)	O(2)−Te(2)−F(7)	90.1(4)	O(3)−Te(3)−F(12)	85.4(4)
O(1)−Te(1)−F(3)	84.2(3)	O(2)−Te(2)−F(8)	89.9(4)	O(3)−Te(3)−F(13)	91.8(4)
O(1)−Te(1)−F(4)	89.2(3)	O(2)−Te(2)−F(9)	84.5(4)	O(3)−Te(3)−F(14)	82.5(3)
O(1)−Te(1)−F(5)	86.0(3)	O(2)−Te(2)−F(10)	85.3(4)	O(3)−Te(3)−F(15)	89.1(4)
F(1)−Te(1)−F(2)	91.4(3)	F(6)−Te(2)−F(7)	92.6(4)	F(11)−Te(3)−F(12)	93.0(4)
F(1)−Te(1)−F(3)	93.9(3)	F(6)−Te(2)−F(8)	92.8(4)	F(11)−Te(3)−F(13)	93.3(3)
F(1)−Te(1)−F(4)	92.8(3)	F(6)−Te(2)−F(9)	92.8(4)	F(11)−Te(3)−F(14)	92.5(4)
F(1)−Te(1)−F(5)	91.4(3)	F(6)−Te(2)−F(10)	92.0(4)	F(11)−Te(3)−F(15)	92.7(4)
F(2)−Te(1)−F(3)	88.7(4)	F(7)−Te(2)−F(8)	89.7(4)	F(12)−Te(3)−F(13)	90.0(3)
F(2)−Te(1)−F(4)	89.7(4)	F(7)−Te(2)−F(9)	90.2(4)	F(12)−Te(3)−F(14)	90.9(3)
F(2)−Te(1)−F(5)	177.1(3)	F(7)−Te(2)−F(10)	175.4(4)	F(12)−Te(3)−F(15)	174.3(4)
F(3)−Te(1)−F(4)	173.2(3)	F(8)−Te(2)−F(9)	174.4(4)	F(13)−Te(3)−F(14)	174.1(4)
F(3)−Te(1)−F(5)	90.7(4)	F(8)−Te(2)−F(10)	90.0(4)	F(13)−Te(3)−F(15)	89.2(3)
F(4)−Te(1)−F(5)	90.6(4)	F(9)−Te(2)−F(10)	89.6(4)	F(14)−Te(3)−F(15)	89.6(3)

$Sb(OTeF_5)_6^-$	CCl_3^+ salt	CBr_3^+ salt	$C(OTeF_5)_3^+$ salt
	bond lengths (Å)		
Sb−O	1.951(3)−1.955(3)	1.936(10)−1.981(10)	1.934(9)−1.957(9)
Te−O	1.844(4)−1.854(3)	1.819(10)−1.868(10)	1.832(9)−1.858(9)
$Te-F_{ax}$	1.834(3)−1.839(3)	1.833(9)−1.852(9)	1.819(8)−1.836(6)
$Te-F_{eq}$	1.819(3)−1.841(3)	1.807(10)−1.849(9)	1.809(7)−1.840(6)
	bond angles (deg)		
Sb−O−Te	137.9(2)−138.2(2)	138.0(6)−140.7(6)	137.2(4)−139.3(4)

SO_2ClF	CBr_3^+ salt	$C(OTeF_5)_3^+$ salt
	bond lengths (Å)	
S−O	1.404(13)−1.417(12)	1.384(11)−1.407(9)
S−F	1.533(10)	1.519(7)−1.520(10)
S−Cl	1.942(7)	1.918(6)−1.951(6)
	bond angles (deg)	
O−S−O	120.9(9)	120.1(7)−122.3(8)
O−S−Cl	109.9(6)−110.0(6)	108.2(5)−111.7(6)
O−S−F	107.0(8)−108.7(7)	106.7(8)−109.4(6)
F−S−Cl	97.8(5)	94.6(5)−99.7(4)

[a] Values in square brackets represent the angles between the pseudo-C_3-axis passing through carbon and the C···F/C···O trajectories.

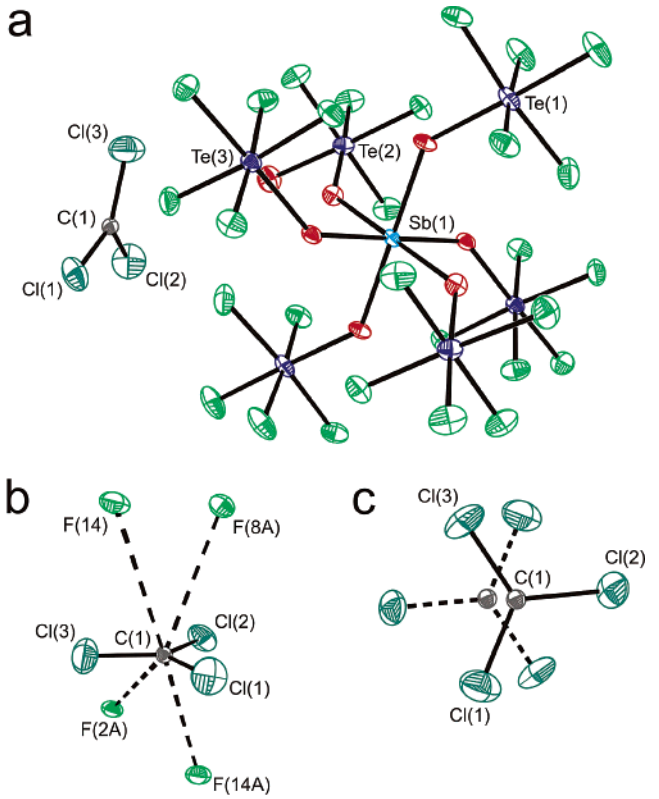

Figure 1. (a) Crystal structure of $[CCl_3][Sb(OTeF_5)_6]$; thermal ellipsoids are shown at the 50% probability level. (b) A view of the CCl_3^+ cation showing the shortest contacts between carbon and the fluorine atoms of the $Sb(OTeF_5)_6^-$ anion. (c) A view of the CCl_3^+ cation, showing the two-fold positional disorder around the crystallographic inversion center.

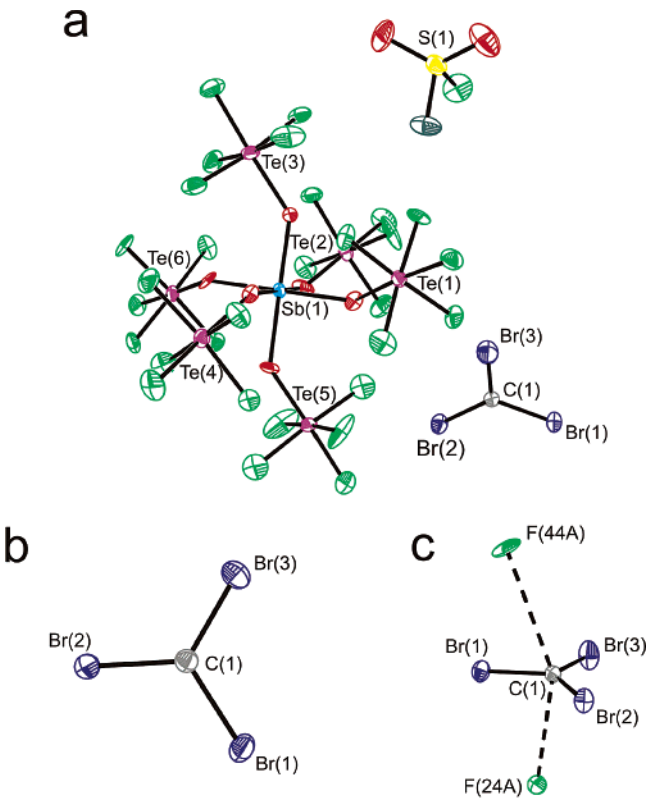

Figure 2. (a) Crystal structure of $[CBr_3][Sb(OTeF_5)_6]\cdot SO_2ClF$; thermal ellipsoids are shown at the 50% probability level. (b) A view of the CBr_3^+ cation, showing the shortest contacts between carbon and the fluorine atoms of the $Sb(OTeF_5)_6^-$ anion.

and CBr_3^+ salts and may be responsible for the absence of disorder in the CBr_3^+ structure.

(b) $[C(OTeF_5)_3][Sb(OTeF_5)_6]\cdot 3SO_2ClF$. The crystal structure of $[C(OTeF_5)_3][Sb(OTeF_5)_6]\cdot 3SO_2ClF$ consists of $Sb(OTeF_5)_6^-$ anions that are well separated from the cations and the solvent molecules, while two of the three SO_2ClF solvent molecules are oxygen coordinated to the carbon atom of the cation (Figure 3).

The $C(OTeF_5)_3^+$ cation is isoelectronic and isostructural with the known $B(OTeF_5)_3$ molecule.[61] To our knowledge, the $C(OTeF_5)_3^+$ cation is only the second example of a trioxygen-substituted carbocation to have been isolated and characterized in the solid state by X-ray crystallography, the first being the AsF_6^- salt of the trigonal planar acidium ion of carbonic acid, $C(OH)_3^+$.[20] The O−C−O angles of the $C(OTeF_5)_3^+$ cation are equal, within $\pm 3\sigma$, to the ideal 120° angle expected for a trigonal planar arrangement. Unlike $B(OTeF_5)_3$ and $C(OH)_3^+$, which have BO_3 and CO_3 arrangements that are planar by symmetry (C_{3h} point symmetry), the planarity of the CO_3 moiety of $C(OTeF_5)_3^+$ is not forced by symmetry, and the three $OTeF_5$ groups bonded to the central carbon atom are crystallographically independent. Despite the low local crystallographic symmetry of $C(OTeF_5)_3^+$ (C_1), the conformational geometry of the cation is very close to the optimized C_{3h} gas-phase geometry of this cation and the known solid-state[61] and calculated gas-phase (see Computational Results for CX_3^+ and BX_3) geometries of $B(OTeF_5)_3$. The tellurium and axial fluorine atoms are slightly out of plane and lie to one side of the CO_3 plane by 0.087 and 0.149 Å, respectively. The C−O bond lengths are similar to those in $C(OH)_3^+$ (1.231(4) Å),[20] $CH_3C(OH)_2^+$ (1.265(6), 1.272(6) Å;[29] 1.261(7), 1.273(7) Å[30]), and $HC(OH)_2^+$ (1.239(6), 1.255(5) Å).[31] As expected for a positively charged isoelectronic species, the C−O bond lengths are shorter than the B−O bond lengths of $B(OTeF_5)_3$ (1.358(6) Å),[61] and the C−O−Te bond angles, which range from 125.7(7) to 132.4(9)°, are similar to those in $B(OTeF_5)_3$ (132.3(4)°).[61] The bond lengths and bond angles in the $OTeF_5$ groups are in good agreement with those observed for the $OTeF_5$ groups of the $Sb(OTeF_5)_6^-$ anion and other $OTeF_5$ derivatives[41,54] and require no further comment.

The $C(OTeF_5)_3^+$ cation has two short C···O contacts [2.690(17) and 2.738(18) Å] with two SO_2ClF solvent molecules (Figure 3, Table 3), which are both nearly perpendicular to the trigonal CO_3 plane, approaching the carbon atoms at angles of 1 and 3° with respect to the pseudo-three-fold symmetry axis of the cation. The contact distances are significantly shorter than the sum of carbon and oxygen van der Waals radii (3.15,[59] 3.20[60] Å) and the C···F contacts in $[CCl_3][Sb(OTeF_5)_6]$ and $[CBr_3][Sb(OTeF_5)_6]\cdot SO_2ClF$, but are similar to the C···F contacts in $[(CH_3)_2CF][AsF_6]$ (2.66(1), 2.78(1) Å) and in $[m\text{-}CF_3C_6H_4)(C_6H_5)CF][AsF_6]$ (2.78(1), 2.79(1) Å). These interactions with the weak Lewis base, SO_2ClF,[62−64] reflect the high positive charge borne by the carbon atom and its substantial Lewis acidity (see Computational Results for CX_3^+ and BX_3).

Raman Spectroscopy. (a) CCl_3^+ and CBr_3^+. The vibrational modes of the CCl_3^+ and CBr_3^+ cations were assigned under

(61) Sawyer, J. F.; Schrobilgen, G. J. *Acta Crystallogr.* **1982**, *B38*, 1561.

(62) Olah, G. A.; Donovan, D. J.; Lin, H. C. *J. Am. Chem. Soc.* **1976**, *98*, 2661.
(63) Calves, J.-Y.; Gillespie, R. J. *J. Am. Chem. Soc.* **1977**, *99*, 1788.
(64) Olah, G. A.; Donovan, D. J. *J. Am. Chem. Soc.* **1978**, *100*, 5163.

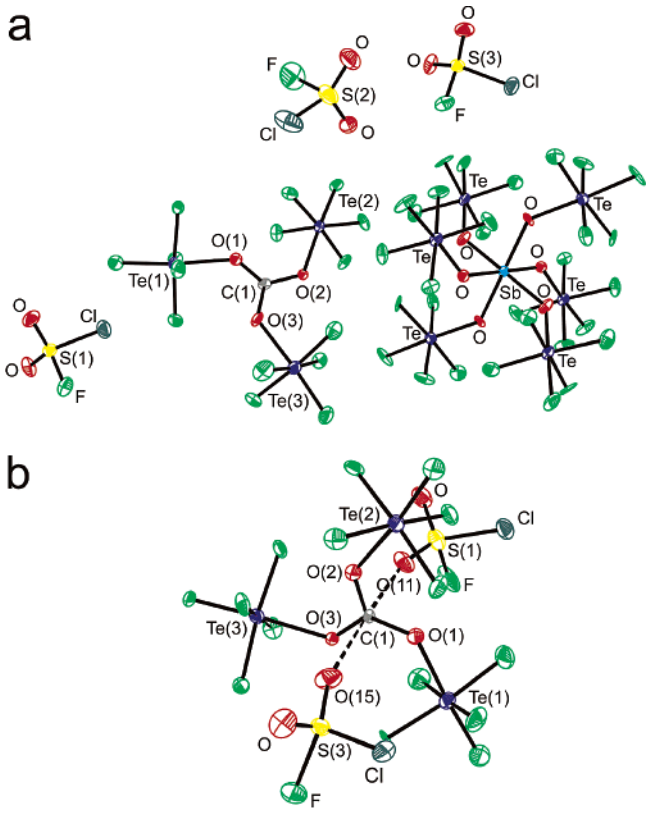

Figure 3. (a) Crystal structure of $[C(OTeF_5)_3][Sb(OTeF_5)_6]\cdot 3SO_2ClF$; thermal ellipsoids are shown at the 50% probability level. (b) A view of the $C(OTeF_5)_3^+$ cation, showing the contacts between the carbon atom and an oxygen atom from each of two SO_2ClF molecules in the crystal lattice.

D_{3h} symmetry and belong to the irreducible representation $\Gamma = A_1' + A_2'' + 2E'$. A total of four fundamental vibrations are expected, $\nu_1(A_1')$, $\nu_2(A_2'')$, $\nu_3(E')$, and $\nu_4(E')$, of which $\nu_1(A_1')$, $\nu_3(E')$, and $\nu_4(E')$ are Raman active and $\nu_2(A_2'')$, $\nu_3(E')$, and $\nu_4(E')$ are infrared active. The Raman assignments for the CCl_3^+ and CBr_3^+ cations were made by comparison with the calculated frequencies and Raman intensities (Table 4), which were carried out at the MP2 level using the basis sets 6-31G(2d) and cc-pVTZ. Calculated frequencies and Raman intensities at the HF level (Table S1) can be found in the Supporting Information. As a benchmark, the vibrational frequencies of CCl_4 and CBr_4 were also calculated with the same basis sets and at the same levels of theory (Table S2).

The low-temperature, solid-state Raman spectra of the solids resulting from the reactions of CCl_4 and CBr_4 with $[XeOTeF_5][Sb(OTeF_5)_6]$ displayed large numbers of bands that could be assigned to the $Sb(OTeF_5)_6^-$ anion, unreacted $XeOTeF_5^+$, and CBr_4 when an excess of CBr_4 was used (Table S3). In the case of CBr_4, new bands were also observed in the S−F, S−O, and C−O stretching regions, which are discussed in the following section. Although the presence of Br_2 could not be ascertained because the expected bands at 296.5 and 302.5 cm^{-1} for solid Br_2[68] overlapped with bands associated with $Sb(OTeF_5)_6^-$ or unreacted $XeOTeF_5^+$, the presence of Br_2 was confirmed by a unit cell determination for solid Br_2 at −173 °C (see Experimental Section). The frequency assignments for the $Sb(OTeF_5)_6^-$ anion and unreacted $XeOTeF_5^+$ cation were made by comparison with those of $[N(CH_3)_4][Sb(OTeF_5)_6]$[41] and $[SbX_4][Sb(OTeF_5)_6]$[54] (X = Cl, Br) and $[XeOTeF_5][AsF_6]$[69] and $[XeOTeF_5][Sb(OTeF_5)_6]\cdot SO_2ClF$,[44] respectively, and require no further comment.

In the CCl_4 system, two new bands were observed at 327 and 554 cm^{-1} which were assigned to $\nu_1(A_1')$ and $\nu_4(E')$ of CCl_3^+, respectively, in excellent agreement with the calculated frequencies and Raman intensities (Table 4). The high-resolution Raman spectrum of $[CCl_3][Sb(OTeF_5)_6]$ reveals that the $\nu_1(A_1')$ band is split into four components that arise from the isotopomers $C^{35}Cl_3^+$, $C^{35}Cl_2{}^{37}Cl^+$, $C^{35}Cl^{37}Cl_2^+$, and $C^{37}Cl_3^+$ (Figure 4). The intensities of the isotopomer bands are in excellent agreement with the intensities calculated from the chlorine natural isotopic abundances. The experimental $^{35}Cl/^{37}Cl$ isotopic shifts are 5.0−5.3 cm^{-1} and are in good agreement with the calculated values (4.8−5.7 cm^{-1}) and are larger than the experimental isotopic shifts of BCl_3 (3.9−4.5 cm^{-1})[67] and CCl_4 (3.2−3.6 cm^{-1}).[70] The formally Raman-active $\nu_3(E')$ band was not observed, in accord with the low Raman intensity calculated for this band at all levels of theory and basis sets used in this study (Table 4).

The low-temperature Raman spectrum resulting from the reaction of CBr_4 with a stoichiometric excess of $[XeOTeF_5][Sb(OTeF_5)_6]$ revealed new bands at 183.5, 187.0, and 321.4 cm^{-1}. The band at 321.4 cm^{-1} is assigned to $\nu_1(A_1')$ of CBr_3^+ by comparison with the calculated value, 340 cm^{-1} (MP2/cc-pVTZ). The intense bands at 183.5 and 187.0 cm^{-1} are assigned to $\nu_4(E')$ of CBr_3^+. The splitting most likely arises from site symmetry lowering of this doubly degenerate mode to produce two Raman-active components. The assignment is supported by the calculated frequency of 186 cm^{-1} (MP2/cc-pVTZ). As in the case of CCl_3^+, the formally Raman-active $\nu_3(E')$ band of CBr_3^+ was not observed. Unlike CCl_3^+, where $\nu_3(E')$ is predicted to be consistently weaker in intensity than $\nu_4(E')$, the relative Raman intensities of $\nu_3(E')$ and $\nu_4(E')$ of CBr_3^+, which are also predicted to be weak, are found to vary with the level of theory and basis set used (Table 4) and are therefore difficult to compare with the experimental Raman intensities. The experimental vibrational frequencies of the CX_3^+ cations are in general found to be comparable to or lower than the calculated values, a better fit being obtained for the MP2 frequencies (Table 4). As expected from the observed and calculated C−X and B−X bond lengths, all frequencies are higher for the CX_3^+ cations than for their BX_3 analogues. The calculated values are also in very good agreement with experimental infrared data obtained for CI_3^+[14] and the matrix-isolated CF_3^+[10] and CCl_3^+[5] cations.

(b) $C(OTeF_5)_3^+$ and $B(OTeF_5)_3$. Although $B(OTeF_5)_3$ has been known for some time and limited infrared data have been previously reported,[71] the Raman spectrum is now reported for the first time (Table 5). The vibrational modes of $B(OTeF_5)_3$ were assigned under C_{3h} symmetry and belong to the irreducible representation $\Gamma = 11A' + 9A'' + 12E' + 8E''$. A total of 40 fundamental bands are expected, of which the 31 A′, E′, and E″ modes are Raman active and the 23 A″ and E′ modes are

(65) Vanderryn, J. *J. Chem. Phys.* **1959**, *30*, 331.
(66) Anderson, T. F.; Lassettre, E. N.; Yost, D. M. *J. Chem. Phys.* **1936**, *4*, 703.
(67) Clark, R. J. H.; Mitchell, P. D. *J. Chem. Phys.* **1972**, *56*, 2225.
(68) Raman spectrum acquired on a sample of solid bromine at −150 °C.
(69) Fir, B. A.; Mercier, H. P. A.; Sanders, J. C. P.; Dixon, D. A.; Schrobilgen, G. J. *J. Fluorine Chem.* **2001**, *110*, 89.
(70) Shurvell, H. F. *Spectrochim. Acta, Part A* **1971**, *27*, 2375.
(71) Kropshofer, H.; Leitzke, O.; Peringer, P.; Sladky, F. O. *Chem. Ber.* **1981**, *114*, 2644.

Table 4. Experimental and Calculated (MP2) Frequencies (cm^{-1}), Raman Intensities[a] and Assignments[b] for CX_3^+ and BX_3 (X = F, Cl, Br, I)

	CF_3^+			BF_3		
assgnts	expt [c]	6-31G(2d)	cc-pVTZ	expt [d]	6-31G(2d)	cc-pVTZ
$\nu_1(A_1')$, $\nu_s(CF_3)$		1048(7)	1072(7)	888.0	883(4)	895(4)
$\nu_2(A_2'')$, $\pi(CF_3)$	798.1	843(0)	825(0)	691.5	723(0)	698(0)
$\nu_3(E')$, $\nu_{as}(CF_3)$	1662.4	1692(<1)	1717(<0)	1453.5	1475(<1)	1484(<1)
$\nu_4(E')$, δ(F−C−F)		595(1)	601(1)	480.4	491(<1)	481(<1)

	CCl_3^+			BCl_3		
assgnts	expt	6-31G(2d)	cc-pVTZ	expt[e]	6-31G(2d)	cc-pVTZ
$\nu_1(A_1')$, $\nu_s(CCl_3)$	554(28)[f]	559(18)	568(17)	467.3	477(9)	483(8)
$\nu_2(A_2'')$, $\pi(CCl_3)$	−	538(0)	541(0)	447.3[i]	465(0)	465(0)
$\nu_3(E')$, $\nu_{as}(CCl_3)$	1035,[g] 1037[h]	1072(<1)	1086(<1)	931	970(<1)	984(<1)
$\nu_4(E')$, δ(Cl−C−Cl)	326.9(9) 187.0(12)	318(4)	317(4)	254.5	257(3)	259(2)

	CBr_3^+			BBr_3		
assgnts	expt	6-31G(2d)	cc-pVTZ	expt[j]	6-31G(2d)	cc-pVTZ
$\nu_1(A_1')$, ν_s(C−Br)	321.4(27)	341(13)	340(13)	279.6	292(7)	292(6)
$\nu_2(A_2'')$, $\pi(CBr_3)$		461(0)	454(0)	377.3[i]	414(0)	401(0)
$\nu_3(E')$, ν_{as}(C−Br)		932(3)	931(2)	794.4	849(<1)	853(<1)
$\nu_4(E')$, δ(Br−C−Br)	183.5(15) 187.0(12)	193(3)	186(3)	153.4	155(1)	157(2)

	CI_3^+		BI_3	
assgnts	expt[k]	(SDB-)cc-pVTZ	expt[j]	(SDB-)cc-pVTZ
$\nu_1(A_1')$, $\nu_s(CI_3)$		240(14)	194.5	203(6)
$\nu_2(A_2'')$, $\pi(CI_3)$	339, w	384(0)	307.9[i]	336(0)
$\nu_3(E')$, $\nu_{as}(CI_3)$	739, vs	807(14)	681	741(<1)
$\nu_4(E')$, δ(I−C−I)		127(3)	105.3	106(2)

[a] Values in parentheses denote experimental uncorrected relative Raman intensities (see Table S3 for anion frequencies and intensities) or calculated Raman intensities (in $Å^4$ amu^{-1}). [b] Frequencies have been calculated and assigned for D_{3h} symmetry. [c] From ref 10. [d] From ref 64. [e] From ref 65. [f] The ν_1 band is split as a result of the mass effect of the ^{35}Cl and ^{37}Cl isotopes: 554.1(100) ($C^{35}Cl_3$), 549.1(96) ($C^{35}Cl_2{}^{37}Cl$), 544.1(32) ($C^{35}Cl^{37}Cl_2$), and 538.8(3) ($C^{37}Cl_3$) cm^{-1}; the most intense band has been scaled to 100 (see Figure 4). [g] From ref 6. [h] From ref 4 and ref 5. [i] Observed as $2\nu_2(A_2'')$. [j] From ref 66. [k] From ref 14.

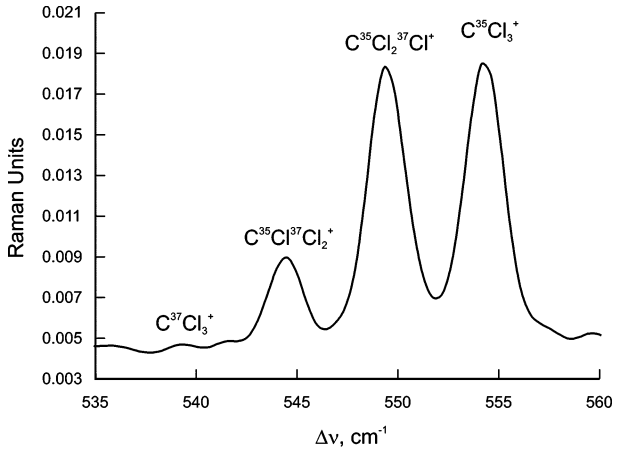

Figure 4. Expanded view of the symmetric $\nu_1(A_1')$ stretching band of CCl_3 in the Raman spectrum of $[CCl_3][Sb(OTeF_5)_6]$, showing the natural abundance chlorine isotope shifts.

infrared active. The vibrational frequencies for $C(OTeF_5)_3^+$ and $B(OTeF_5)_3$ were calculated at the HF level using the (SDB)-cc-pVTZ basis set. The assignments for $B(OTeF_5)_3$ were made by comparison with the calculated frequencies and infrared and Raman intensities, which are in agreement with the experimental values (Table 5).

The low-temperature spectra resulting from the reaction of CBr_4 with a 2-fold molar excess of $[XeOTeF_5][Sb(OTeF_5)_6]$ revealed new bands in the high-frequency stretching region. The majority of these bands can be assigned to coordinated (see X-ray Crystal Structures) and non-coordinated (frequencies in square brackets) SO_2ClF:[44] $\nu_{asym}(SO_2)$, 1415, 1407 [1444, 1433, 1427] cm^{-1}; $\nu_{sym}(SO_2)$, 1166 [1224, 1219] cm^{-1}, and ν(SF), 819 [839] cm^{-1} (Table S3). Although the bands at 1095 and 1454 cm^{-1} fall in the range of the calculated $\nu_{sym}(CO_3)$ and $\nu_{asym}(CO_3)$ frequencies for $C(OTeF_5)_3^+$, 1165 and 1502 cm^{-1} (HF/(SDB)-cc-pVTZ), they could not be definitively assigned to the $C(OTeF_5)_3^+$ cation but could also be associated with the mixed Br/$OTeF_5$-substituted cations, $CBr(OTeF_5)_2^+$ and $CBr_2(OTeF_5)^+$, formed in eqs 3−5.

Computational Results for CX_3^+ and BX_3 (X = F, Cl, Br, I, $OTeF_5$). Quantum mechanical ab initio calculations have been previously reported for the isoelectronic CX_3^+ [6,12,14,34,37,72−79] and BX_3,[14,34,80−85] (X = F, Cl, Br, I) series and related isovalent species such as AH_2X^+, YH_2X (X = F, Cl, Br, I; A = C, Si, Ge, Sn, Pb; Y = B, Al, Ga, In, Tl).[34] While results are abundant for species where X = F[14,72,74−77,80−85] or Cl,[14,37,72,78−87] they are relatively sparse for X = Br,[12,14,37,72] or I.[12,14,37]

(72) Reynolds, C. H. *J. Chem. Soc., Chem. Commun.* **1991**, 975.
(73) Dixon, D. A.; Feller, D.; Sandrone, G. *J. Phys. Chem. A* **1999**, *103*, 4744.
(74) Ricca, A. *J. Phys. Chem. A* **1999**, *103*, 1876.
(75) Hansel, A.; Scheiring, C.; Glantschnig, M.; Lindinger, W.; Ferguson, E. E. *J. Chem. Phys.* **1998**, *109*, 1748.
(76) Irikura, K. K. *J. Am. Chem. Soc.* **1999**, *121*, 7689.
(77) Basch, H.; Hoz, T.; Hoz, S. *J. Phys. Chem. A* **1999**, *103*, 6458.
(78) Rodriquez, C. F.; Bohme, D. K.; Hopkinson, A. C. *J. Phys. Chem.* **1996**, *100*, 2942.
(79) Robles, E. S. J.; Chen, P. *J. Phys. Chem.* **1994**, *98*, 6919.
(80) Jonas, V.; Frenking, G.; Reetz, M. T. *J. Am. Chem. Soc.* **1994**, *116*, 8741.
(81) Chandrakumar, K. R. S.; Pal, S. *J. Phys. Chem. A* **2002**, *106*, 11775.
(82) Rowsell, B. D.; Gillespie, R. J.; Heard, G. L. *Inorg. Chem.* **1999**, *38*, 4659.
(83) Bauschlicher, C. W. J.; Ricca, A. *J. Phys. Chem. A* **1999**, *103*, 4313.
(84) Fau, S.; Frenking, G. *Mol. Phys.* **1999**, *96*, 519.
(85) Brinck, T.; Murray, J. S.; Politzer, P. *Inorg. Chem.* **1993**, *32*, 2622.

Table 5. Calculated[a] Vibrational Frequencies (cm^{-1}) and Infrared and Raman Intensities for $C(OTeF_5)_3^+$ and $B(OTeF_5)_3$ and Observed Vibrational Frequencies and Infrared and Raman Intensities for $B(OTeF_5)_3$

$C(OTeF_5)_3^+$	$B(OTeF_5)_3$			
calcd[b–d] (C_{3h})	calcd[b–d] (C_{3h})	expt Raman	expt infrared[e]	assgnt (C_{3h})
1502 (0.2) [1266.5]	1297 (0.1) [1095.2]		1330, s	E′
1165 (0.7) [i.a.]	1066 (3.5) [i.a.]	1050(6)		A′
798 (i.a.) [316.7]	758 (i.a.) [484.5]		740, vs	A″
785 (0.1) [101.4]	754 (0.3) [272.7]	755(5)		E′
780 (0.1) [179.2]	770 (0.6) [92.4]			E′
779 (0.2) [i.a.]	751 (0.2) [i.a.]			E″
777 (i.a.) [133.6]	658 (i.a.) [2.7]			A″
777 (1.3) [i.a.]	749 (1.5) [i.a.]	732(5)		A′
764 (11.6) [i.a.]	731 (21.1) [i.a.]	716(96)		A′
755 (2.0) [112.9]	716 (1.4) [78.8]		725, vs	E′
712 (32.9) [i.a.]	683 (17.3) [i.a.]	673(100)		A′
708 (0.3) [0.8]	674 (1.2) [7.2]	702(16)	705, s	E′
682 (2.8) [i.a.]	660 (2.7) [i.a.]	660(18)		E″
680 (i.a.) [1.0]	626 (i.a.) [73.6]		615, m	A″
448 (7.5) [i.a.]	474 (10.2) [i.a.]	500(44)		A′
388 (0.1) [98.4]	430 (0.0) [125.3]		430, s	E′
346 (0.1) [i.a.]	355 (0.1) [i.a.]	338(7)		A′
331 (0.0) [i.a.]	342 (0.0) [i.a.]	332(3)		E″
328 (i.a.) [191.3]	337 (i.a.) [189.9]			A″
325 (2.3) [i.a.]	328 (0.0) [i.a.]			A′
325 (0.5) [5.1]	332 (0.7) [46.7]	325(15)		E′
321 (0.6) [92.2]	327 (0.1) [236.3]			E′
317 (0.0) [i.a.]	315 (2.0) [i.a.]	318(17)		A′
311 (1.0) [i.a.]	327 (1.3) [i.a.]	311(18)		E″
308 (0.0) [293.9]	314 (0.3) [0.2]			E′
303 (i.a.) [0.0]	319 (i.a.) [3.9]			A″
260 (0.1) [i.a.]	256 (0.3) [i.a.]	254(3)		A′
254 (0.7) [0.3]	247 (0.5) [11.7]	246(7)		E′
216 (0.2) [i.a.]	216 (0.0) [i.a.]			E″
207 (i.a.) [0.0]	214 (i.a.) [0.1]			A″
198 (0.0) [i.a.]	210 (0.0) [i.a.]			E″
198 (i.a.) [0.0]	206 (i.a.) [0.6]			A″
140 (0.3) [i.a.]	143 (0.2) [i.a.]	140(3)		A′
129 (0.1) [0.4]	129 (0.1) [1.1]			E′
88 (0.1) [i.a.]	77 (0.0) [i.a.]	71(5)		A′
77 (0.1) [i.a.]	63 (0.1) [i.a.]	56(3)		E″
35 (0.0) [0.3]	29 (0.0) [0.1]			E′
28 (i.a.) [0.2]	24 (i.a.) [0.1]			A″
20 (i.a.) [0.3]	15 (i.a.) [0.0]			A″
20 (0.0) [i.a.]	16 (0.2) [i.a.]			E″
		159(2)		lattice modes
		98(2), 91(3)		
		84(5)		

[a] HF/(SDB-)cc-pVTZ; calculated frequencies have been scaled by multiplying the calculated frequencies by 0.890. [b] Raman intensities, in $Å^4$ amu^{-1}, are given in parentheses. [c] Infrared intensities, in km mol^{-1}, are given in square brackets. [d] The abbreviation, i.a., denotes an inactive mode. [e] Experimental values are from ref 70 (KBr, −195 °C). The abbreviations denote very strong (vs), strong (s), and medium (m) infrared intensities.

The series of trihalomethyl carbocations, CX_3^+, and boron trihalides, BX_3, (X = F, Cl, Br, I) have been reinvestigated, and the calculations have been extended to the related $OTeF_5$ derivatives using all-electron correlation consistent (cc-pVTZ) basis sets for all atoms other than tellurium and iodine, for which semi-relativistic large core pseudopotential ((SDB)-cc-pVTZ) basis sets were used. The geometric parameters and vibrational frequencies (see Raman Spectroscopy) were calculated, and a natural bond orbital (NBO) analysis was carried out at the HF and MP2 levels of theory. Energies for the MP2-optimized structures were calculated at the QCISD(T) level. Calculations for the $OTeF_5$ derivatives were only carried out at the HF level (see Experimental Section) using the (SDB)-cc-pVTZ basis set. The methods were benchmarked by calculating the vibrational frequencies (Table S2), geometries (Table S4), and chemical shifts of CX_4 (see Chemical Shifts and Coupling Constant Trends) for which there are well-established experimental values.

(a) Geometries. Geometry optimization using D_{3h} (CX_3^+ and BX_3), and C_{3h} ($C(OTeF_5)_3^+$, $B(OTeF_5)_3$) as the initial symmetries resulted in stationary points with all frequencies real. All optimized metric parameters for CX_3^+ and BX_3 are listed in Tables 6 and 7, respectively.

The HF and MP2 calculations give essentially the same results for CCl_3^+, CBr_3^+, CI_3^+, and the isoelectronic BX_3 molecules, while for CF_3^+ and BF_3, the MP2 calculations predict slightly longer bond lengths. The calculated bond lengths of CCl_3^+, CBr_3^+, and CI_3^+ are in good agreement with those obtained from their X-ray crystal structures. The calculated bond lengths for all BX_3 molecules are also in good agreement with experiment and the experimental bond length trends, C−X < B−X, are reproduced for X = Cl, Br, I.

The fully optimized (HF/(SDB)-cc-pVTZ) geometries of $C(OTeF_5)_3^+$ and $B(OTeF_5)_3$ possess C_{3h} symmetry (Figure 5), with trigonal planar environments around the central carbon and boron atoms. The calculated distances are in reasonable agreement with the experimental ones, although they are all slightly shorter. The calculated C−O−Te, B−O−Te, and $OTeF_5$ group angles are in good agreement with the observed angles. Overall, the calculated geometries are in very good agreement with the experimental geometries of the $C(OTeF_5)_3^+$ cation and $B(OTeF_5)_3$, indicating that the two C···O contacts with two SO_2ClF solvent molecules in the crystal lattice of $[C(OTeF_5)_3][Sb(OTeF_5)_6]\cdot 3SO_2ClF$ do not have a significant effect on the structure of the cation in the solid state (see X-ray Crystal Structures). Moreover, the small distortions of the F−Te−F bond angles from 90° in $C(OTeF_5)_3^+$ and the near-regular $OTeF_5$ groups observed for $B(OTeF_5)_3$ are also reproduced by the calculations.

(b) Natural Bond Orbital (NBO) Analyses. Natural atomic charges, Mayer natural atomic orbital valencies, and natural atomic orbital bond orders between atoms in CX_3^+, CX_4, and BX_3, calculated at the MP2 level of theory, are given in Table S5 and those calculated for $C(OTeF_5)_3^+$ and $B(OTeF_5)_3$, at the HF level of theory, are given in Table 8. Natural atomic orbital (NAO) populations (Table S6) are given in the Supporting Information.

(i) B−X/C−X σ- and π-Donations and Natural Atomic Charges. Following previous approaches, bonding at the central carbon and boron atoms was divided into σ- and π-donation, and the values obtained agreed well with the previous values and associated interpretations (see Tables 8 and S5).[26,34]

The NBO analyses for CX_3^+ and BX_3 (X = F or $OTeF_5$) were carried out at the same level of theory (HF/(SDB-)cc-pVTZ; see Tables 8 and S6), so that both the carbocations and neutral boron analogues could be compared. The π-donations from the fluorine or from the oxygen atom of the $OTeF_5$ ligand to the central carbon or boron atom are similar for CX_3^+ (0.15 for X = F; 0.19 for X = $OTeF_5$), and BX_3, (0.09 for X = F or $OTeF_5$). In both cases, the σ-donation from the carbon or boron atom to the ligand atom decreases when fluorine is replaced by the $OTeF_5$ group. The charge on the carbon atom of $C(OTeF_5)_3^+$ (1.30) is lower than that on the carbon atom of CF_3^+ (1.57),

(86) Hudgens, J. W.; Johnson, R. D. I.; Tsai, B. P.; Kafafi, S. A. *J. Am. Chem. Soc.* **1990**, *112*, 5763.
(87) Tachikawa, H. *J. Phys. Chem. A* **1997**, *101*, 7454.

Table 6. Experimental and Calculated Geometries for CX_3^+ and BX_3

CF_3^+		6-31G(2d)		cc-pVTZ			BF_3		6-31G(2d)		cc-pVTZ		
		HF	MP2	HF	MP2	CCSD(T)		expt[a]	HF	MP2	HF	MP2	CCSD(T)
C−F (Å)	1.209	1.236	1.208	1.233	1.233	B−F (Å)	1.30(2)	1.294	1.315	1.295	1.315	1.313
F−C−F (deg)	120					F−B−F (deg)		120				
F···F (Å)	2.095	2.141	2.093	2.135	2.136	F···F (Å)	2.26(3)	2.241	2.277	2.243	2.277	2.274

CCl_3^+		6-31G(2d)		cc-pVTZ			BCl_3		6-31G(2d)		cc-pVTZ		
	expt[b]	HF	MP2	HF	MP2	CCSD(T)		expt[c]	HF	MP2	HF	MP2	CCSD(T)
C−Cl (Å)	1.62(1)	1.645	1.654	1.641	1.645	1.655	B−Cl (Å)	1.75(2)	1.750	1.750	1.747	1.740	1.747
Cl−C−Cl (deg)	119.9(7)	120					Cl−B−Cl (deg)		120				
Cl···Cl (Å)	2.805(5)	2.848	2.865	2.842	2.849	2.866	Cl···Cl (Å)	2.99(3)[a]	3.031	3.031	3.025	3.015	3.026

CBr_3^+		6-31G(2d)		cc-pVTZ			BBr_3			6-31G(2d)		cc-pVTZ	
	expt[b]	HF	MP2	HF	MP2	CCSD(T)		expt	HF	MP2	HF	MP2	CCSD(T)
C−Br (Å)	1.81(2)	1.800	1.803	1.808	1.801	1.816	B−Br (Å)	1.893(5)[d]	1.896	1.888	1.910	1.891	1.901
Br−C−Br (deg)	120.0(9)	120					Br−B−Br (deg)		120				
Br···Br (Å)	3.129(3)	3.117	3.123	3.132	3.120	3.145	Br···Br (Å)	3.25(3)[a]	3.284	3.270	3.308	3.275	3.293

CI_3^+		(SDB)-cc-pVTZ			BI_3		(SDB)-cc-pVTZ		
	expt[e]	HF	MP2	CCSD(T)		expt	HF	MP2	CCSD(T)
C−I (Å)	2.013(9)	2.001	1.990	2.007	B−I (Å)	2.112(8)[f]	2.117	2.092	2.105
I−C−I (deg)	120.0(5)				I−B−I (deg)	120.0(9)	120		
I··· I (Å)	3.486(8)	3.466	3.447	3.477	I···I (Å)	3.659[f]	3.667	3.624	3.646

[a] From ref 87. [b] Average values, present work. [c] From ref 88. [d] From ref 89. [e] From ref 14. [f] From ref 90, the I···I contact distance was calculated from the published coordinates.

Table 7. Calculated[a] and Experimental Geometries for $C(OTeF_5)_3^+$ and $B(OTeF_5)_3$

$C(OTeF_5)_3^+$ (C_{3h})	expt[b]	calcd	$B(OTeF_5)_3$ (C_{3h})	expt[c]	calcd
		bond lengths (Å)[d]			
C(1)−O(1)	1.28(3)	1.256	B(1)−O(1)	1.358(6)	1.354
Te(1)−O(1)	1.98(1)	1.945	Te(1)−O(1)	1.874(6)	1.833
Te(1)−F(1)	1.81(1)	1.765	Te(1)−F(1)	1.822(6)	1.785
Te(1)−F(2)	1.81(2)	1.778	Te(1)−F(2)	1.809(4)	1.790
Te(1)−F(3)	1.81(2)	1.771	Te(1)−F(3)	1.818(4)	1.785

$C(OTeF_5)_3^+$ (C_{3h})	expt[b]	calcd	$B(OTeF_5)_3$ (C_{3h})	expt[c]	calcd
		bond angles (deg)[d]			
C(1)−O(1)−Te(1)	129.8(1)	135.27	B(1)−O(1)−Te(1)	132.3(4)	137.32
O(1)−Te(1)−F(1)	175.9(6)	180.00	O(1)−Te(1)−F(1)	178.0(3)	180.00
O(1)−Te(1)−F(2)	90.2(9)	88.43	O(1)−Te(1)−F(2)	92.6(2)	91.88
O(1)−Te(1)−F(3)	84.7(9)	85.50	O(1)−Te(1)−F(3)		89.56
F(1)−Te(1)−F(2)	92.6(9)	92.75	F(1)−Te(1)−F(2)	88.8(2)	89.12
F(1)−Te(1)−F(3)	92.6(9)	93.32	F(1)−Te(1)−F(3)	89.0(2)	89.44
F(2)−Te(1)−F(3)	89.9(9)	89.76	F(2)−Te(1)−F(3)	90.2(2)	89.87
F(2)−Te(1)−F(4)	90.0(9)	89.68	F(2)−Te(1)−F(4)	91.2(2)	90.12
F(2)−Te(1)−F(5)	174.8(9)	173.92	F(2)−Te(1)−F(5)		178.56

[a] HF/(SDB-)cc-pVTZ. [b] Experimental values are averaged values. [c] From ref 60. [d] The atom numbering scheme corresponds to that of the equivalently labeled $OTeF_5$ group of the $C(OTeF_5)_3^+$ cation in Figure 3, where F(1) is the axial fluorine and F(2−5) are the equatorial fluorines. In the calculated structure, the F(2)/F(4) and the F(3)/F(5) pairs are related by symmetry.

and the overall charge of the $OTeF_5$ group (−0.10) is somewhat lower than that of fluorine in CF_3^+ (−0.12). The lower positive charge on the carbon atom of $C(OTeF_5)_3^+$ is consistent with the lower electronegativity of the $OTeF_5$ group.[92] In both $C(OTeF_5)_3^+$ and $B(OTeF_5)_3$, the charges on the central atom are lower and that on the ligand is more positive when compared with the atomic charges of CF_3^+ and BF_3, respectively.

(ii) Mayer Bond Orders and Natural Atomic Orbital Valencies for $C(OTeF_5)_3^+$ and $B(OTeF_5)_3$. The B−O bond order and valencies at the boron and oxygen atoms are lower for $B(OTeF_5)_3$ than the corresponding values of $C(OTeF_5)_3^+$,

(88) Lévy, H.; Brockway, L. O. *J. Am. Chem. Soc.* **1937**, *59*, 2085.
(89) Spencer, C.; Lipscomb, W. N. *J. Chem. Phys.* **1958**, *28*, 355.
(90) Konaka, S.; Ito, T.; Morino, Y. *Bull. Chem. Soc. Jpn.* **1966**, *39*, 1146.

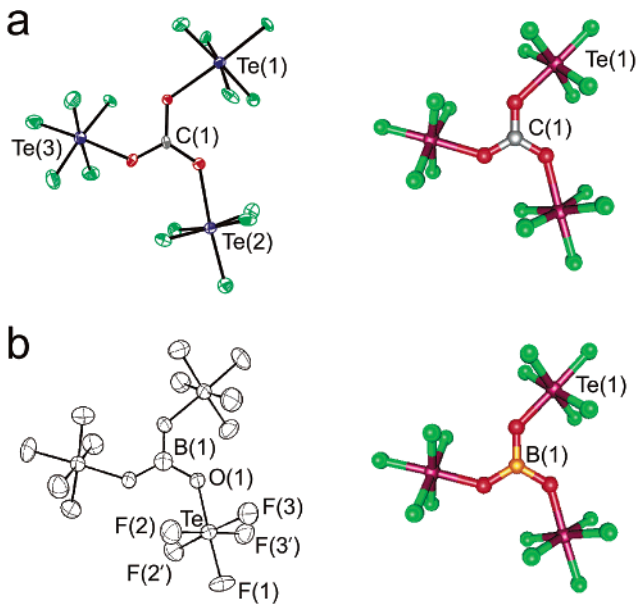

Figure 5. Experimental (left) and calculated (right) geometries for (a) the $C(OTeF_5)_3^+$ cation and (b) the $B(OTeF_5)_3$ molecule (experimental structure from ref 61).

indicating somewhat less double bond character. These observations are also reflected in the π donation which is lower for B←O (0.09) than for C←O (0.19). At the HF level, the B−F bond order and valencies at boron and fluorine are also lower for BF_3 than the corresponding values for CF_3^+. The difference between the valencies at boron in BF_3 and in $B(OTeF_5)_3$ is 0.35, which is almost the same as the difference between the valencies at carbon in CF_3^+ and in $C(OTeF_5)_3^+$, 0.38. These trends indicate that the electronic properties of $C(OTeF_5)_3^+/CF_3^+$ and $B(OTeF_5)_3/BF_3$ are similar.

Chemical Shift and Coupling Constant Trends. The ^{13}C chemical shifts of the CCl_3^+ and CBr_3^+ cations are significantly deshielded with respect to their parent tetrahalomethanes (Table 1). The ^{13}C resonance of CI_3^+ has also been shown to be strongly deshielded with respect to CI_4 (Table 9).[12,13] Electronic structure calculations (MP2/(SDB-)cc-pVTZ) reveal that the ^{13}C deshielding that results from carbocation formation, $\Delta\delta(^{13}C)$, parallels the decrease in the natural atomic charge on carbon relative to the carbon charge in the tetrahalide (Table S5). This reduction in negative charge (CCl_3^+, 0.10; CBr_3^+, 0.10; CI_3^+, 0.26) does not, however, fully account for the extent of deshielding, $\Delta\delta(^{13}C)$ (CCl_3^+, +140.7 ppm; CBr_3^+, +239.4 ppm; CI_3^+, +389.3 ppm), observed in the ^{13}C NMR spectra. The shielding changes can be rationalized in terms of the paramagnetic shielding contribution (σ^p) to the overall screening of the ^{13}C nucleus (σ) in the Ramsey equation (eq 13),

$$\sigma = \sigma^p + \sigma^d \qquad (13)$$

where σ^d is the diamagnetic shielding contribution. The paramagnetic term in the Ramsey equation is negative and can be interpreted in terms of the atom-in-a-molecule approach as defined in eq 14,

Table 8. Calculated[a] Natural Atomic Charges, Mayer Bond Orders, and Mayer Natural Atomic Orbital Valencies for $C(OTeF_5)_3^+$ and $B(OTeF_5)_3$

$C(OTeF_5)_3^+$ (C_{3h})[b]	charge	valency		bond order
C	1.30	3.04	C−O	1.01
O	−0.86	1.33	Te−O	0.45
Te	4.07	3.19	Te−F_A	0.56
F_A	−0.65	0.53	Te−F_B	0.54
F_B	−0.67	0.49	Te−$F_{B'}$	0.55
$F_{B'}$	−0.66	0.51		
overall $OTeF_5$	−0.10			
p_π populations at C (O)			0.56 (1.80)	
σ donation (π donation)[c]			0.28 (0.19)	

CF_3^+ (D_{3h})	charge	valency		bond order
C	1.57	2.66	C−F	0.89
F	−0.19	0.82		
p_π populations at C (F)			0.46 (1.83)	
σ donation (π donation)[c]			0.34 (0.15)	

$B(OTeF_5)_3$ (C_{3h})[b]	charge	valency		bond order
B	1.45	2.18	B−O	0.73
O	−1.15	1.22	Te−O	0.58
Te	4.08	3.22	Te−F_A	0.53
F_A	−0.68	0.49	Te−F_B	0.52
F_B	−0.68	0.48	Te−$F_{B'}$	0.53
$F_{B'}$	−0.68	0.49		
overall $OTeF_5$	−0.48			
p_π populations at B (O)			0.27 (1.88)	
σ donation (π donation)[c]			0.57 (0.09)	

BF_3 (D_{3h})	charge	valency		bond order
B	1.56	2.53	B−F	0.84
F	−0.52	0.80		
p_π populations at B (F)			0.26 (1.91)	
σ donation (π donation)[c]			0.61 (0.09)	

[a] HF/(SDB-)cc-pVTZ. [b] The symbols, F_A and $F_B/F_{B'}$ denote axial and equatorial fluorine atoms, where F_B and $F_{B'}$ are nonequivalent under C_{3h} symmetry. [c] The value given is per bond; a negative sign indicates donation in reversed order.

$$\sigma_p \approx -\left(\frac{\mu_o}{4\pi}\right)\left(\frac{4\mu_B^2}{\Delta E}\right)[\langle r^{-3}\rangle_{np} P_i + \langle r^{-3}\rangle_{nd} D_i] \qquad (14)$$

where μ_o is the magnetic moment for a given nucleus, μ_B is the Bohr magneton, ΔE is the mean excitation energy, $\langle r^{-3}\rangle_{np}$ and $\langle r^{-3}\rangle_{nd}$ are the inverse cube roots of the mean expectation values for the p and d orbital distances from the nucleus, and P_i and D_i are the degrees of imbalance of valence electrons in p and d orbitals, respectively. The approach, a one-center approximation, is restricted to terms centered on the nucleus in question. As the bond length contracts in going from the neutral halide (Table S4) to the cation (Table 6), the mean expectation value of the inverse cube of the 2p orbital radius of carbon in eq 14 is expected to increase. The bond length contraction and concomitant increase in $\langle r^{-3}\rangle_{2p}$ results in a more negative paramagnetic contribution to the overall nuclear magnetic shielding term of carbon and, in turn, to a high-frequency ^{13}C chemical shift. Similar trends are noted for the isoelectronic boron trihalides, BX_3,[94] and the tetrahaloborates, BX_4^- (X = F, Cl, Br, I).[97]

There are significant discrepancies between the experimental ^{11}B and ^{13}C NMR chemical shifts of BX_3 and CX_3^+ and those

(91) Albert, B.; Schmitt, K. *Z. Anorg. Allg. Chem.* **2001**, *627*.
(92) Birchall, T.; Myers, R. D.; de Waard, H.; Schrobilgen, G. J. *Inorg. Chem.* **1982**, *21*, 1068.
(93) DeMarco, R. A.; Fox, W. B.; Moniz, W. B.; Sojka, S. A. *J. Magn. Reson.* **1975**, *18*, 522.

Table 9. Experimental and Calculated[a] Chemical Shifts for CX_3^+ and BX_3 (X = F, Cl, Br, I, $OTeF_5$) and CX_4 (X = F, Cl, Br, I)

	^{13}C[b]			^{19}F[c]		
	expt	6-31G(d)[d,e]	cc-pVTZ[d,e]	expt	6-31G(d)[d,e]	cc-pVTZ[d,e]
CF_3^+	− (150.7)[f]	155.5	154.5	−	32.1	32.9
CCl_3^+	237.1[d] (236.3)[g]	249.8	254.8			
CBr_3^+	209.7[d] (207)[g]	304.9	312.8			
CI_3^+	97[h] (95)[g]		436.4			

	^{13}C[b]		^{19}F[c]	
	expt[d]	SDB-cc-pVTZ[d,e]	expt[d]	SDB-cc-pVTZ[d,e]
$C(OTeF_5)_3^+$	168.8	139.5	−57.6 (F_A) −31.6 (F_B)	−132.7 (F_A) −107.3 (F_B)

	^{13}C[b]			^{19}F[c]		
	expt	6-31G(d)[d,e]	cc-pVTZ[d,e]	expt[d]	6-31G(d)[d,e]	cc-pVTZ[d,e]
CF_4	(119.9)[i]	119.6	123	−62.4	−88.8	−76.2
CCl_4	96.4[d]	132.1	137			
CBr_4	−29.7[d]	139.1	142			
CI_4	−292.3[j]	−	93			

	^{11}B[k]		^{19}F[c]	
	expt[l,m]	SDB-cc-pVTZ[d,e]	expt[m]	SDB-cc-pVTZ[d,e]
$B(OTeF_5)_3$	−22.9	75.4	−48.2 (F_A) −44.4 (F_B)	−62.8 (F_A) −53.4 (F_B)

	^{11}B[k]			^{19}F[c]		
	expt[n]	6-31G(d)[d,e]	cc-pVTZ[d,e]	expt	6-31G(d)[d,e]	cc-pVTZ[d,e]
BF_3	10.0	30.8	24.0	−126.8[o]	−132.5	−125.6
BCl_3	46.5	73.1	68.8	−		
BBr_3	38.7	92.8	73.1	−		
BI_3	−7.9		117.8	−		

[a] Chemical shifts were calculated at the B3LYP/6-311G(d)//HF/6-31G(d) and B3LYP/(SDB-)cc-pVTZ//HF/(SDB-)cc-pVTZ levels for CX_3^+, CX_4 and BX_3, and at the B3LYP/(SDB-)cc-pVTZ//HF/(SDB-)cc-pVTZ level for $C(OTeF_5)_3^+$ and $B(OTeF_5)_3$. [b] Referenced to TMS. [c] Referenced to $CFCl_3$. [d] Present work. [e] The predicted chemical shifts reported here have been obtained by subtracting their absolute values from that of their respective reference compound, i.e., TMS (^{13}C), 180.9969 ppm (T_d, 6-311G*) and 181.2543 ppm (T_d, (SDB-)cc-pVTZ); $CFCl_3$ (^{19}F), 167.9485 ppm (C_{3v}, 6-311G*) and 183.9397 ppm (C_{3v}, (SDB-)cc-pVTZ); $F_3BO(C_2H_5)_2$ (^{11}B), 123.7710 ppm (C_{3v}, 6-311G*) and 116.3587 ppm (C_{3v}, cc-pVTZ). [f] From ref 13. [g] From ref 12. [h] From ref 14. [i] ^{13}C From ref 92. [j] From ref 93. [k] referenced to $B(OCH_3)_3$. [l] The ^{11}B chemical shift quoted in the literature (ref 70) was referenced to $B(OCH_3)_3$ and converted to the ^{11}B chemical shift referenced to $F_3BO(C_2H_5)_2$ by subtraction of 18.3 ppm. [m] From ref 70. [n] The ^{11}B spectra were recorded in methyl cyclohexane at 33.5 °C (ref 94). [o] From ref 95.

calculated by the GIAO method (B3LYP/(SDB-)cc-pVTZ) for the heavier halides (Table 9). The calculated ^{11}B and ^{13}C NMR chemical shifts show monotonic increases from BCl_3 to BI_3 and from CCl_3^+ to CI_3^+ (inverse halogen effects), which contrast with the observed trends of decreasing chemical shift upon descending group 17 (Table 9). The calculated chemical shift trends arise from larger paramagnetic contributions expected for increasingly more covalent interactions between the central atom and the halogen atom upon descending group 17. The discrepancies between the calculated and experimental chemical shifts, however, result from neglect of the effect of spin−orbit (SO) coupling on the overall nuclear shielding, which is not taken into account by the original Ramsey equation.[98] Spin−orbit coupling causes a triplet excitation on the heavy atom, which, in turn, is transmitted to a neighboring atom through the bond. As previously shown, inclusion of the SO-correction increases the shielding calculated for boron and carbon bonded to bromine or iodine and results in good agreement with observed ^{11}B and ^{13}C NMR chemical shifts for the BX_3[99] and CX_3^+ [37] series. Although plots of ^{11}B and ^{13}C chemical shifts versus halogen electronegativity for BX_4,[97] BX_3,[97] CX_4,[100] and CX_3^+ [13] are near linear for X = Cl, Br, and I, it has been pointed out that such trends are fortuitous, and are, in fact, attributable to the SO coupling term.[37] The ^{11}B chemical shift of BF_3 and the predicted ^{13}C chemical shift of CF_3^+ cannot be understood in terms of the high electronegativity of fluorine, nor can they be understood in terms of the traditional notion that high shielding arises from p(π) back-donation to the boron[101,102] or carbon[12] atom from the fluorine atoms. Electronic structure calculations, however, reveal that the p(π) back-bonding components in BF_3 and CF_3^+ are weakest among their respective trihalide series (Table S5). Thus, the increased shieldings experienced by the boron and carbon nuclei are actually the normal behavior and arise from the highly ionic characters of the B−F and C−F bonds, which lead to large ΔE values and smaller paramagnetic contributions to their respective nuclear shieldings (eq 14).[37,99]

The ^{13}C chemical shift of $C(OTeF_5)_3^+$ (168.8 ppm) is in good agreement with values reported for other peroxygen-substituted

(94) Lappert, M. F.; Litzow, M. R.; Pedley, J. B.; Tweedale, A. *J. Chem. Soc. A* **1971**, 2426.
(95) Branchadell, V.; Oliva, A. *J. Mol. Struct. (THEOCHEM)* **1991**, *236*, 75.
(96) Coyle, T. D.; Stone, F. G. A. *J. Chem. Phys.* **1960**, *32*, 1892.
(97) Hartman, S.; Schrobilgen, G. J. *Inorg. Chem.* **1972**, *11*, 940.
(98) Morishima, I.; Endo, K.; Yonezawa, T. *J. Chem. Phys.* **1973**, *59*, 3356.
(99) Kaupp, M. Relativistic Effects on NMR Chemical Shifts. In *Relativistic Electronic Structure Theory II: Applications*; Schwerdtfeger, P., Ed; Elsevier: Amsterdam, 2004. In press.
(100) Malkin, V. G.; Malkina, O. L.; Salahub, D. R. *Chem. Phys. Lett.* **1996**, *261*, 335.
(101) Onak, T.; Landesman, H.; Williams, R. E.; Shapiro, I. *J. Phys. Chem.* **1959**, *63*, 1533.

carbocations ($C(OH)_3^+$, 166.8 ppm;[20] $C(OCH_3)OH_2^+$, 164.1 ppm[19]). The experimental carbon deshielding relative to that of $C(OTeF_5)_4$ ($\Delta\delta(^{13}C)$, 53.0 ppm) is consistent with cation formation, and follows the trend predicted for CF_3^+/CF_4 ($\Delta\delta(^{13}C)$, 30.8 ppm). This result indicates that the C−O bonding in $C(OTeF_5)_3^+$ is highly ionic, as expected from the estimated high electronegativity of the $-OTeF_5$ group (3.87),[92] leading to a small paramagnetic contribution to the overall nuclear shielding and, thus, to a relatively shielded ^{13}C nucleus. This ionic character is supported by electronic structure calculations (HF/(SDB-)cc-pVTZ; vide supra) which show that the charge on the carbon of the $C(OTeF_5)_3^+$ cation (+1.30) is nearly equal to that of CF_3^+ (+1.37), which is consistent with the ^{13}C NMR empirically predicted (150.7 ppm)[13] and calculated (167.9, 169.2 ppm;[13] 154.5 ppm, this work) ^{13}C chemical shifts for the CF_3^+ cation.

The ^{13}C resonance of $CBr(OTeF_5)_2^+$ was observed at 187.6 ppm, but that of $CBr_2(OTeF_5)^+$ was not observed. The chemical shift of $CBr_2(OTeF_5)^+$ was predicted from pairwise additivity relationships (eq 15),[97,103]

$$\delta = \sum \eta_{i,j} \tag{15}$$

where $\eta_{i,j}$ is a parameter associated with the carbon substituents i and j and independent of all other substituents. The pairwise additivity parameters $\eta_{Br,Br}$ (69.9 ppm), $\eta_{OTeF_5,OTeF_5}$ (56.3 ppm), and $\eta_{Br,OTeF_5}$ (65.6 ppm) were evaluated from the experimental chemical shifts of CBr_3^+, $CBr(OTeF_5)_2^+$, and $C(OTeF_5)_3^+$. In this way, the chemical shift of $CBr_2(OTeF_5)^+$ is predicted to be 201.1 ppm from eq 16.

$$\delta(^{13}C) = \eta_{Br,Br} + 2\eta_{Br,OTeF_5} \tag{16}$$

The ^{19}F NMR data for $CBr_n(OTeF_5)_{3-n}^+$ are provided in Table 1. Previous attempts have been made to correlate the ^{19}F NMR trends observed for the $OTeF_5$ group in different chemical environments.[45,104] The trends observed in the present study are in good agreement with the previously noted trends in ^{19}F chemical shift and $^2J(^{19}F_A-^{19}F_B)$; however, some significant differences occur for $OTeF_5$ bound to carbocation centers: (1) The ^{19}F chemical shifts of the equatorial fluorine environments of $CBr_n(OTeF_5)_{3-n}^+$ have a substantially broader chemical shift range (−31.6 to −19.9 ppm) than the axial fluorine environments (−61.3 to −57.6 ppm), contrasting with the ranges observed for neutral ($^{19}F_B$, −56.6 to −36.7 ppm; $^{19}F_A$, −54.6 to −27.8 ppm) $OTeF_5$-substituted compounds.[104] (2) The $^2J(^{19}F_A-^{19}F_B)$ values range from 156 to 164 Hz, which is significantly smaller than the previously observed range for neutral and anionic species (175−195 Hz).[104] Moreover, the decrease in coupling in going from the neutral species to the cation also holds for $BrOTeF_5$ (180 Hz) and the $Br(OTeF_5)_2^+$ cation (164 Hz). (3) The $^1J(^{19}F_A-^{123,125}Te)$ and $^1J(^{19}F_B-^{123,125}Te)$ couplings increase substantially in going from $C(OTeF_5)_4$ to $C(OTeF_5)_3^+$, from $CBr(OTeF_5)_2^+$ to $CBr_2(OTeF_5)^+$, and from $BrOTeF_5$ to $Br(OTeF_5)_2^+$ (Table 1). Furthermore, the magnitude of the coupling increases to the greatest extent on going from $C(OTeF_5)_3^+$ to $CBr_2(OTeF_5)^+$. Although there are no other systematic studies involving $OTeF_5$ ligands bound to a cation center, these observations are consistent with cation formation, and the trends across the $CBr_n(OTeF_5)_{3-n}^+$ series can be correlated with increasing covalent character of the C−O bond with increasing bromine substitution.

Conclusions

The present study provides a new oxidative route to carbocations and the first solid-state characterization of the previously reported CCl_3^+ and CBr_3^+ cations as well as that of the novel $C(OTeF_5)_3^+$ cation. The cations have been stabilized as salts of the preformed, oxidatively resistant, and weakly coordinating $Sb(OTeF_5)_6^-$ anion, which avoids the use of more strongly coordinating anions derived from strong Lewis acid ligand acceptors, such as SbF_5. Despite their anticipated high electrophilicity, these salts have appreciable stabilities at or near room temperature. In addition, the $CBr(OTeF_5)_2^+$ and $Br(OTeF_5)_2^+$ cations and $C(OTeF_5)_4$ have been characterized by ^{13}C and/or ^{19}F NMR spectroscopy. NMR spectroscopy has also been used to monitor carbocation formation, ligand substitution by means of redox elimination, and decomposition pathways in these systems.

X-ray crystallographic studies show, in all cases, that the carbocation center is planar in the absence of symmetry constraints imposed by the crystal lattice. Despite the strong Lewis acidities predicted for perhalomethyl cations, the CCl_3^+ and CBr_3^+ cations are well isolated in their respective crystal lattices and possess only long secondary C···F contacts to fluorine atoms of the $Sb(OTeF_5)_6^-$ anion that do not significantly exceed the sum of the van der Waals radii of carbon and fluorine. Secondary X···F and X···O (X = Cl, Br) contacts that are close to the sums of the van der Waals radii of the halogen and an oxygen atom of cocrystallized SO_2ClF or a fluorine atom of the anion exist for CCl_3^+ and CBr_3^+ that are in accord with the calculated positive charges on the halogen atoms of both cations.

Computational studies reproduce the experimental metric parameters of CCl_3^+, CBr_3^+, and $C(OTeF_5)_3^+$, and the vibrational frequencies of CCl_3^+ and CBr_3^+, and have been extended to their $-OTeF_5$ derivatives.

Contrasting with the CCl_3^+ and CBr_3^+ cations, the $C(OTeF_5)_3^+$ cation possesses two short C···O contacts to the oxygen atoms of two weakly basic, cocrystallized SO_2ClF molecules, which is consistent with the high positive charge on carbon predicted by electronic structure calculations, and which approximates the positive charge calculated for the highly Lewis acidic CF_3^+ cation.

Experimental Section

Apparatus and Materials. Manipulations of volatile materials were carried out on a glass vacuum line, while nonvolatile materials were handled inside a drybox as previously described.[54] All reaction vessels were fabricated from $^1/_4$-in. o.d. FEP tubing, joined to Kel-F valves by means of compression fittings, and were dried under vacuum for several hours prior to passivation with 1 atm of fluorine gas for 8−12 h. All vacuum-line connections were made by use of $^1/_4$-in. stainless steel Cajon Ultratorr unions fitted with Viton O-rings. Sulfuryl chloride fluoride, SO_2ClF, (Allied Chemical) was purified by use of the literature method.[105] Carbon tetrachloride (BDH Chemicals) was dried for several days over CaH_2 and distilled into a glass vessel fitted with a 4-mm J.

(102) Good, C. D.; Ritter, D. M. *J. Am. Chem. Soc.* **1962**, *84*, 1162.
(103) Vladimiroff, T.; Malinowski, E. R. *J. Chem. Phys.* **1967**, *46*, 1830.
(104) Seppelt, K. *Angew. Chem., Int. Ed. Engl.* **1982**, *21*, 877.
(105) Schrobilgen, G. J.; Holloway, J. H.; Granger, P.; Brevard, C. *Inorg. Chem.* **1978**, *17*, 980.

Young glass/Teflon stopcock prior to use. Carbon tetrabromide (Aldrich) was purified by sublimation at ca. 60 °C under dynamic vacuum. The compound, $BrOTeF_5$, was prepared and purified as previously described.[43] The synthesis and structural characterization of $[XeOTeF_5][Sb(OTeF_5)_6]$ will be described in a forthcoming publication.[44] Because $[XeOTeF_5][Sb(OTeF_5)_6]$ undergoes decomposition at temperatures approaching ambient, the compound was manipulated inside a drybox using low-temperature procedures as previously described.[106]

Raman Spectroscopy. (a) Raman Sample Preparation. (i) $[CCl_3][Sb(OTeF_5)_6]$. Inside the drybox, 0.07141 g (0.0371 mmol) of $[XeOTeF_5][Sb(OTeF_5)_6]$ at −120 °C was transferred by use of a precooled syringe for solids into a 25-cm long $^1/_4$-in. o.d. FEP reaction vessel maintained at −120 °C. The cold reaction vessel was closed with a Kel-F valve, and the contents were then removed from the drybox, immediately placed in a −78 °C bath, and connected to a glass vacuum line, where SO_2ClF solvent (ca 1.5 mL) was condensed into the reaction vessel under static vacuum at −196 °C. A stoichiometric amount of CCl_4 vapor (470 Torr, 0.00586 g, 0.0381 mmol) was measured into a calibrated bulb (1.488 mL) and then condensed into the reactor under static vacuum at −196 °C. Warming to −78 °C resulted in rapid reaction which was indicated by a color change from a bright yellow to a colorless solution and by evolution of xenon gas. The solvent was removed under vacuum at −78 °C, and the Raman spectrum of the resulting white powder was acquired.

(ii) $[CBr_3][Sb(OTeF_5)_6]$ and $[C(OTeF_5)_3][Sb(OTeF_5)_6]$. Inside the drybox, 0.06860 g (0.0357 mmol) of $[XeOTeF_5][Sb(OTeF_5)_6]$ and 0.01666 g (0.0503 mmol) of CBr_4 were loaded into a $^1/_4$-in. o.d. FEP reaction vessel at −120 °C. The valved reaction vessel and contents were then removed cold from the drybox and immediately placed in a −78 °C bath and connected to a glass vacuum line, where SO_2ClF solvent (ca 1.5 mL) was condensed into the reactor under static vacuum. Upon warming, the reaction proceeded rapidly at −78 °C to give xenon gas and a red-brown solution, which changed over time (ca. 4−5 h) to a red-orange solution. The solvent was removed under vacuum at −78 °C, and the Raman spectrum of the resulting white powder was acquired.

(b) Raman Instrumentation and Spectral Acquisition. The low-temperature (−160 °C) Raman spectra of microcrystalline samples resulting from the reaction of CCl_4 and CBr_4 with $[XeOTeF_5][Sb(OTeF_5)_6]$ were recorded on a Bruker RFS 100 FT Raman spectrometer using 1064-nm excitation and a resolution of 1 cm^{-1} as previously described.[106] The spectra were recorded using a laser power of 300 mW and a total of 1200 scans.

Nuclear Magnetic Resonance Spectroscopy. (a) NMR Sample Preparation. All NMR samples were prepared in 5-mm o.d. thin wall precision glass NMR tubes (Wilmad) fused to $^1/_4$-in. o.d. lengths of glass tubing which were in turn attached to 4-mm J. Young Teflon stopcocks by use of $^1/_4$-in. stainless steel Cajon Ultratorr unions fitted with Viton O-rings. The NMR tubes were then vacuum-dried for 8−12 h before use. Reactions between $[XeOTeF_5][Sb(OTeF_5)_6]$ and the starting reagent(s) were carried out in SO_2ClF solvent at −78 °C for ca. 2 h. The NMR tubes were then flame sealed under dynamic vacuum at −196 °C and stored at the same temperature prior to acquisition of the NMR spectra.

(i) $[CX_3][Sb(OTeF_5)_6]$ (X = Cl, Br, $OTeF_5$). Stoichiometric amounts of solid $[XeOTeF_5][Sb(OTeF_5)_6]$ (0.04134 g, 0.0215 mmol) and CBr_4 (0.01091 g, 0.0329 mmol) were weighed into an NMR tube in the drybox and transferred to a glass vacuum line, where 0.4−0.5 mL of SO_2ClF was vacuum distilled onto the mixture at −78 °C. To enhance the yield of $[C(OTeF_5)_3][Sb(OTeF_5)_6]$, $BrOTeF_5$ was condensed onto the sample of $[CBr_3][Sb(OTeF_5)_6]$ (see eqs 2−6) in a 3:1 mole ratio based on initial amounts of $[XeOTeF_5][Sb(OTeF_5)_6]$ and CBr_4 and allowed to react at −20 °C for ca. 3 h. In the case of CCl_4 (270 Torr, 0.00337 g, 0.0219 mmol), SO_2ClF was vacuum distilled onto $[XeOTeF_5][Sb(OTeF_5)_6]$ (0.04152 g, 0.02159 mmol), followed by condensation of CCl_4 onto the mixture at −196 °C.

(ii) $C(OTeF_5)_4$. Inside the drybox, 0.05568 g (0.1679 mmol) of solid CBr_4 was transferred to an NMR tube, followed by removal from the drybox and connection to a glass vacuum line, where SO_2ClF solvent (0.4−0.5 mL) was statically distilled under vacuum onto the solid at −78 °C. A stoichiometric amount of $BrOTeF_5$ (0.21818 g, 0.6850 mmol) was then vacuum distilled into the sample tube at −196 °C.

(iii) $[Br(OTeF_5)_2][Sb(OTeF_5)_6]$. Inside the drybox, $[XeOTeF_5][Sb(OTeF_5)_6]$ (0.10124 g, 0.05264 mmol) was transferred at −120 °C to an NMR sample tube kept at the same temperature. The sample was removed from the drybox, immediately cooled to −78 °C, and connected to a glass vacuum line, and 0.4−0.5 mL of SO_2ClF was condensed onto the sample under static vacuum at −78 °C. A stoichiometric excess of $BrOTeF_5$ (0.02347 g, 0.0737 mmol) was then vacuum distilled into the tube at −196 °C.

(b) NMR Intrumentation and Spectral Acquisition. Nuclear magnetic resonance spectra were recorded unlocked (field drift < 0.1 Hz h^{-1}) on a Bruker DRX-500 spectrometer equipped with an 11.744 T cryomagnet. For low-temperature work, the NMR probe was cooled using a nitrogen flow and variable-temperature controller (BV-T 3000).

The ^{19}F (^{13}C) NMR spectra were obtained using a 5-mm combination $^1H/^{19}F$ (broad-band inverse) probe operating at 470.592 (125.758) MHz. The spectra were recorded in 64 (32) K memories, with a spectral width setting of 24 (38) kHz, yielding a data point resolution of 0.36 (1.15) Hz/data point and acquisition times of 1.39 (0.436) s. A relaxation delay of 0.1 (1−10) s was applied, and 2000 (1000−10000) transients were typically accumulated using a pulse width of 2.5 (6) μs, corresponding to a bulk magnetization tip angle, θ, of approximately 90°. A line-broadening of 0.7 (5) Hz was used in the exponential multiplication of the free induction decays prior to Fourier transformation. The ^{19}F and ^{13}C NMR spectra were referenced externally at 30 °C to samples of neat $CFCl_3$ and TMS, respectively. The chemical shift convention used is that a positive (negative) sign indicates a chemical shift to high (low) frequency of the reference compound.

X-ray Crystallography. (a) Crystal Growth of $[CCl_3][Sb(OTeF_5)_6]$, $[CBr_3][Sb(OTeF_5)_6]\cdot SO_2ClF$, and $[C(OTeF_5)_3][Sb(OTeF_5)_6]\cdot 3SO_2ClF$. Crystals of $[CCl_3][Sb(OTeF_5)_6]$ were obtained by reaction of ca. 0.2 g of $[XeOTeF_5][Sb(OTeF_5)_6]$ and a 2-fold molar excess of CCl_4 in 1.5 mL of SO_2ClF inside a T-shaped $^1/_4$-in. o.d. FEP reaction vessel. Crystals were grown by slow cooling of the reaction mixture from −20 to −50 °C over a period of 6 h inside the vertical arm of the reaction vessel. Colorless, plate-shaped crystals were isolated by decanting the solvent into the horizontal arm, followed by drying under dynamic vacuum at −78 °C. The crystals were mounted as previously described.[106] Crystals of $[CBr_3][Sb(OTeF_5)_6]\cdot SO_2ClF$ (pale yellow), $[C(OTeF_5)_3][Sb(OTeF_5)_6]\cdot 3SO_2ClF$ (colorless), and Br_2 (red brown) crystals were grown and isolated in a manner analogous to that described above for $[CCl_3][Sb(OTeF_5)_6]$. Bromine was identified by determination of the unit cell parameters[107,108] at −173 °C for a crystal selected from the bulk sample.

(b) Crystal Mounting and X-ray Data Collection. All crystals were mounted at −100 ± 3 °C as previously described,[106] and centered on a P4 Siemens diffractometer, equipped with a Siemens SMART 1K CCD area detector, controlled by SMART,[109] and a rotating anode emitting Kα radiation monochromated (λ = 0.71073 Å) by a graphite crystal. Diffraction data collection (−173 °C) consisted of a full ψ-rotation at $\chi = 0°$ (using 1040 + 30) 0.3° frames, followed by a series of short (100 frames) ω scans at various ψ and χ settings to fill the gaps. The crystal-to-detector distance was 5.012 cm, and the data

(106) Gerken, M.; Dixon, D. A.; Schrobilgen, G. J. *Inorg. Chem.* **2000**, *39*, 4244.
(107) Vonnegut, B.; Warren, B. E. *J. Am. Chem. Soc.* **1936**, *58*, 2459.
(108) Powell, B. M.; Heal, K. M.; Torrie, B. H. *Mol. Phys.* **1984**, *53*, 929.
(109) *SMART*, release 5.054, and *SAINT*, release 6.01; Siemens Energy and Automation Inc.; Madison, WI, 1999.

collection was carried out in a 512 × 512 pixel mode using 2 × 2 pixel binning. Processing of the raw data was completed using SAINT+,[109] which applied Lorentz and polarization corrections to three-dimensionally integrated diffraction spots. The program SADABS[110] was used for the scaling of diffraction data, the application of a decay correction, and an empirical absorption correction on the basis of the intensity ratios of redundant reflections.

(c) Solution and Refinement of the Structure. The XPREP[111] program was used to confirm the unit cell dimensions and the crystal lattices. The solutions were obtained by direct methods, which located the positions of the atoms defining the $Sb(OTeF_5)_6^-$ anions, the CBr_3^+ and $C(OTeF_5)_3^+$ cations and SO_2ClF molecules. In the case of the CCl_3^+ salt, the difference Fourier map was obtained after solutions by direct methods revealed a trigonal planar CCl_3^+ cation positioned close to the inversion center, which gave rise to a two-fold positional disorder. The site occupancy factors of all the atoms defining the CCl_3^+ cation were therefore set to 0.5. The final refinement was obtained by introducing anisotropic thermal parameters and the recommended weight for most of the atoms. The maximum electron densities in the final difference Fourier map were located near the heavy atoms.

All calculations were performed using the SHELXTL-plus package[111] for the structure determination and solution refinement and for the molecular graphics.

Calculations. Electronic structure calculations were carried out at the HF, MP2 (for geometry optimizations, Natural Bond Orbital analysis, vibrational frequencies and intensities) and CCSD(T) (for single-point energies at the MP2 geometries) levels of theory using the program Gaussian-98 (version A-11).[112] The standard all-electron 6-31G(2d) and cc-pVTZ basis sets as implemented in the Gaussian program were utilized for all elements except Te and I, for which the semirelativistic large core (RLC) pseudopotential basis set (SDB-)cc-pVTZ was used. The combined use of cc-pVTZ and (SDB-)cc-pVTZ basis sets is indicated as (SDB-)cc-pVTZ. Nuclear magnetic resonance shielding tensors were calculated at the B3LYP/6-311G(d)//HF/6-31G-(d) and B3LYP/(SDB-)cc-pVTZ//HF/(SDB-)cc-pVTZ levels using gauge-independent atomic orbital method (GIAO) as implemented in Gaussian 98.

Natural orbital analyses were performed using HF or MP2 densities with the NBO program (versions 3.1 and 5.0).[113] The use of a pseudopotential basis set instead of an all-electron basis set was tested, and the overall results did not differ significantly, as pointed out previously.[114]

Acknowledgment. This paper is dedicated to our friend and colleague Professor Ronald J. Gillespie on the occasion of his 80th birthday and in recognition of his many outstanding contributions across a broad spectrum of chemistry. We thank the Natural Sciences and Engineering Research Council (NSERC) of Canada for the award of a postgraduate scholarship (M.D.M.) and for support in the form of a research grant (G.J.S.). We also thank the Finnish IT Center for Science for the use of their computing resources (R.J.S.) and Prof. K. O. Christe for helpful discussions relating to the preparation of this manuscript.

Supporting Information Available: Experimental and calculated Raman frequencies and intensities for CX_3^+ and BX_3 (X = F, Cl, Br, I) at the HF and MP2 levels (Table S1). Experimental and calculated Raman frequencies and intensities for CX_4 (X = F, Cl, Br, I) (Table S2). Raman frequencies and assignments for $[CCl_3][Sb(OTeF_5)_6]$ and $[CBr_3][Sb(OTeF_5)_6]$ and related species (Table S3). Experimental and calculated geometrical parameters and NBO study for CX_4 (X = F, Cl, Br, I) (Table S4). Calculated natural atomic charges, Mayer bond orders, and Mayer natural atomic orbital valencies for CX_3^+, CX_4, and BX_3 (X = F, Cl, Br, I) (Table S5). Valence NAO populations for CX_3^+ and BX_3 (X = F, Cl, Br, I, $OTeF_5$) and CX_4 (X = F, Cl, Br, I) (Table S6). The X-ray crystallographic files in CIF format for the structure determinations of $[CCl_3][Sb(OTeF_5)_6]$, $[CBr_3][Sb(OTeF_5)_6]\cdot SO_2ClF$, and $[C(OTeF_5)_3][Sb(OTeF_5)_6]\cdot 3SO_2ClF$. This material is available free of charge via the Internet at http://pubs.acs.org.

JA030649E

(110) Sheldrick, G. M. SADABS (Siemens Area Detector Absorption Corrections), personal communication, 1998.
(111) *SHELXTL-Plus*, release 5.1; Siemens Analytical X-ray Instruments, Inc.: Madison, WI, 1998.
(112) Frisch, M. J.; Trucks, G. W.; Schlegel, H. B.; Scuseria, G. E.; Robb, M. A.; Cheeseman, J. R.; Zakrzewski, V. G.; Montgomery, J. A., Jr.; Stratmann, R. E.; Burant, J. C.; Dapprich, S.; Millam, J. M.; Daniels, A. D.; Kudin, K. N.; Strain, M. C.; Farkas, O.; Tomasi, J.; Barone, V.; Cossi, M.; Cammi, R.; Mennucci, B.; Pomelli, C.; Adamo, C.; Clifford, S.; Ochterski, J.; Petersson, G. A.; Ayala, P. Y.; Cui, Q.; Morokuma, K.; Salvador, P.; Dannenberg, J. J.; Malick, D. K.; Rabuck, A. D.; Raghavachari, K.; Foresman, J. B.; Cioslowski, J.; Ortiz, J. V.; Baboul, A. G.; Stefanov, B. B.; Liu, G.; Liashenko, A.; Piskorz, P.; Komaromi, I.; Gomperts, R.; Martin, R. L.; Fox, D. J.; Keith, T.; Al-Laham, M. A.; Peng, C. Y.; Nanayakkara, A.; Challacombe, M.; Gill, P. M. W.; Johnson, B.; Chen, W.; Wong, M. W.; Andres, J. L.; Gonzalez, C.; Head-Gordon, M.; Replogle, E. S.; Pople, J. A.; *Gaussian 98*, Revision A.11; Gaussian, Inc.: Pittsburgh, PA, 2001.
(113) (a) Reed, A. E.; Weinstock, R. B.; Weinhold, F. *J. Chem. Phys.* **1985**, *83*, 735. (b) Reed, A. E.; Curtiss, L. A.; Weinhold, F. *Chem. Rev.* **1988**, *88*, 899. (c) Glendening, E. D.; Reed, A. E.; Carpenter, J. E.; Weinhold, F. *NBO*, Version 3.1; Gaussian, Inc.: Pittsburgh, PA, 1990. (d) Glendening, E. D.; Badenhoop, J. K.; Reed, A. E.; Carpenter, J. E.; Bohmann, C. M.; Morales, C. M.; Weinhold, F. *NBO*, Version 5.0; Theoretical Chemistry Institute, University of Wisconsin, Madison, WI, 2001.
(114) Simón-Manso, Y.; Fuentealba, P. *J. Mol. Struct. (THEOCHEM)* **2003**, *634*, 89.